DOI: 10.26599/FSHW.2026.9250965

W.L. Yang et al. / Food Science and Human Wellness 16 (2027)

Contents lists available at SciOpen

Food Science and Human Wellness

journal homepage: https://www.sciopen.com/journal/2097-0765

China Food Publishing Co.

Procyanidin B2 improves insulin resistance by regulating the IRS1/PI3K/AKT-Nrf2-GSK3β based on computational biology, molecular evidence and direct binding proof

Wenli Yang[1], Shiyun Chen[1], Rong Tong[1], Yuhang Yi[3], Dongsheng Wang[2], Fangfang Yan[1], Tao Li[4*], Chenghao Lv[2, 3*], Si Qin[1, 2, 3*]

[1] *College of Food Science and Technology, Hunan Agricultural University, Changsha 410128, China;*

[2] *Institute of Integrative Medicine, Hunan Provincial Key Laboratory of Liver Visceral Manifestation in Traditional Chinese Medicine, Department of Integrated Traditional Chinese and Western Medicine, Xiangya Hospital, Central South University, Changsha 410008, China;*

[3] *College of Bioscience and Biotechnology, Hunan Agricultural University, Changsha 410128, China;*

[4] *Hunan Agricultural Products Processing Institute, Hunan Academy of Agricultural Sciences, Changsha 410125, China.*

ABSTRACT: Procyanidin B2 (PB2), a dimer of oligomeric procyanidins, has been reported to ameliorate abnormal glucose metabolism; however, its efficacy in regulating redox-related insulin resistance (IR) and underlying mechanism has not yet been studied. Currently, antioxidant activity and digestive enzyme inhibitory tests were applied to screen the preliminary chemopreventive effect of PB2 on glucose metabolism dysfunction, further computational biology and molecular verification to elucidate its mechanism on improving IR. The results indicated that PB2 had limited antioxidant property against ROS and inhibitory property on digestive enzyme. Network pharmacology analysis implied that PI3K/AKT and FoxO pathways were the main targeted by PB2 to combating IR. Further molecular data demonstrated that PB2 promoted glycogen synthesis by activation of PI3K/AKT-Nrf2 signaling pathway via promoting posttranscriptional protein stability, nuclear translocation of Nrf2 and ARE binding ability, and inhibited gluconeogenesis by stimulating FoxO1 phosphorylation to reduce the expression of downstream G6Pase. Innovatively, molecular docking coupled with different Pull-Down assays revealed that PB2 could directly bind with AKT, Nrf2 and GSK3β, suggesting PB2 may improve IR via regulation of PI3K/AKT-Nrf2-GSK3β signaling, more than FoxO1 signaling pathway; subsequently, Nrf2 could directly bind with GSK3β, reinforcing evidence for PB2-Nrf2-GSK3β complex formation. Besides, co-treatment with PI3K/AKT and Nrf2 inhibitors or siRNAs highlighted the essential role of Nrf2 activation in PB2-contributed IR improvement. Moreover, PB2 has also been validated to exert its effect via regulation of PI3K/AKT-Nrf2-GSK3β signaling pathway *in vivo*. Therefore, these findings suggest that PB2 is a potent and promising compound to ameliorate glucose metabolism by targeting IR.

Keywords: procyanidin B2; insulin resistance; network pharmacology; molecular docking; PI3K/AKT-Nrf2-GSK3β signaling

1. Introduction

Diabetes is the most typical chronic metabolic disease besides obesity, which is usually accompanied by cardiovascular, renal, neuropathic, and retinopathic complications, among others[1]. The International

***Corresponding author**
litao@hunaas.cn (T.L.); lvchenghao0514@163.com (C.L.); qinsiman@hunau.edu.cn (S.Q.)

Received 15 April 2025
Received in revised from 29 June 2025
Accepted 22 October 2025

Diabetes Federation predicts that there will be 592 million diabetes patients globally by 2035, and 90% of them will suffer from type 2 diabetes mellitus (T2DM). T2DM is marked by insufficient insulin secretion and insulin resistance (IR)[2]. IR is marked by reduced insulin sensitivity in target tissues such as the liver, muscle, and adipose tissue, impairing insulin's capacity to regulate glucose metabolism. As a core feature of T2DM, IR precedes T2DM and persists through the disease[3]. Therefore, improving IR is considered a persuasive treatment strategy for T2DM.

The liver is a vital target for insulin, responsible for maintaining and regulating insulin signals. Insulin receptor substrate 1 (IRS1) plays a critical role in liver insulin signaling, while activation of the phosphoinositide 3-kinase (PI3K)/protein kinase B (AKT) pathway boosts insulin signaling and receptor sensitivity[4][5]. Additionally, there is evidence to suggest that AKT, a crucial molecule in insulin signaling, enhances glucose transporter 4 (GLUT4), regulates forkhead box protein O1 (FoxO1), and modulates glycogen synthase kinase-3β (GSK3β) expression, thereby facilitating cellular glucose utilization[6]. AKT also suppresses gluconeogenesis by inhibiting key enzymes like glucose-6-phosphatase (G6Pase), and regulates GSK3β activity to facilitate glycogen synthesis[7][8]. Furthermore, nuclear factor erythroid 2-related factor 2 (Nrf2), which is a powerful antioxidant against oxidative stress, can activate phase II detoxifying enzyme system when oxidative stress occurs. This activation accelerates the clearance of free radicals and alleviates IR[9][10]. However, the potential of PB2 to ameliorate IR through activation of the PI3K/AKT/Nrf2/GSK3β and FoxO1 signaling pathways remains unclear.

Research has indicated that various natural compounds isolated from vegetables, fruits, grains, and herbs exhibit proven hypoglycemic effects[11][12], and they hold potential as valuable sources for the development of antidiabetic medications. Procyanidins are polyphenolic compounds found in many plants, found abundantly in grapes, cranberries, and other berries, and effectively address T2DM prevention and treatment[13]. Certain studies have indicated that procyanidins can enhance lipid metabolism in T2DM by inhibiting fat production and improving mitochondrial function[14]. Cranberry procyanidins can alleviate obesity and hyperlipidemia caused by high-fat/high sugar intake in C57BL/6J mice, inhibit fat production in the liver, stimulate fatty acid beta-oxidation, and reduce the expression of key enzymes involved in hepatic gluconeogenesis[15]. Procyanidins protect diabetes nephropathy induced by cadmium via p38 MAPK and Keap1/Nrf2 signaling pathways[16]. Procyanidin B2 (PB2) is a common dimer of oligomeric procyanidins. PB2 alleviates lipid irregularities, hyperglycemia, and oxidative stress in metabolic syndrome patients via its antioxidant capabilities. Additionally, it can mitigate diet-induced obesity and non-alcoholic fatty liver disease by modulating rabbit gut microbiota[17]. PB2 can reduce glucose digestion and absorption by inhibiting digestive enzyme activity. The study by Han et al. showed that PB2 has an inhibitory effect on α-glucosidase and this process is a reversible mixed inhibition mode[18]. Dai et al. found that PB2 can reduce intrinsic fluorescence and surface hydrophobicity of α-amylase, and spontaneously form complexes[19]. Although the protective effect of PB2 in metabolic disorders has been partially confirmed, the specific

molecular mechanism by which it improves IR, especially whether it involves the synergistic regulation of insulin signaling and antioxidant pathways remains unclear.

Therefore, this study investigates whether PB2 enhances insulin sensitivity via modulating of the PI3K/AKT/Nrf2/GSK3β and FoxO1 signaling pathways, with dual objectives of characterizing the molecular mechanisms underlying PB2-mediated amelioration of IR and establishing a pharmacological basis for developing PB2-based interventions against diabetes mellitus and its pathophysiological sequelae.

2. Materials and methods

2.1 Materials and reagents

PB2 (CAS no.29106-49-8; purity≥98%) was purchased from Weikeqi Biotechnology Co., Ltd. (Sichuan, China). Acarbose, α-glucosidase, p-nitrophenyl-α-D-glucoside (pNPG, 99.9%), α-amylase, and metformin (MET) were acquired from Yuanye Bio-Technology Co., Ltd. (Shanghai, China). Fetal bovine serum (FBS) was obtained from Viva Cell Biosciences Ltd. (Shanghai, China), while trypsin was purchased from Biosharp (Beijing, China). Phosphate-buffered saline (PBS) was obtained from Boster (Wuhan, China). Glucosamine (GlcN) was sourced from Sigma-Aldrich (St. Louis, US). The Nrf2 inhibitor ML385 was obtained from Selleck Chemicals (Houston, USA), and the PI3K/AKT inhibitor LY294002 was purchased from Abmole Bioscience (Houston, USA). Kits for glucose oxidase-peroxidase, superoxide dismutase (SOD), malondialdehyde (MDA), glutathione (GSH), Catalase (CAT), triglycerides (TG), total cholesterol (TC), high-density lipoprotein cholesterol (HDL-C), and low-density lipoprotein cholesterol (LDL-C), Aspartate Aminotransferase (AST), Alanine Aminotransferase (ALT) were sourced from Nanjing Jiancheng Bioengineering Institute (Nanjing, China). BCA Protein Quantification Kit, RIPA lysate, Gel-shift™ Chemiluminescent electrophoretic mobility shift assay (EMSA) kit were purchased from Beyotime Institute of Biotechnology (Shanghai, China). GST PullDown assay kit was purchased from ThermoFisher Scientific (Lenexa, KS). Primary antibodies targeting IRS1, p-IRS1, AKT, p-AKT, GSK3β, p-GSK3β, Nrf2, FoxO1, p-FoxO1, NADPH quinone oxidoreductase (NQO1), and heme oxygenase-1 (HO-1) were obtained from Cell Signaling Technology (Beverly, USA). Primary antibodies for GLUT4, G6Pase, and GAPDH, as well as secondary antibodies against mouse and rabbit, were sourced from Proteintech Group (Wuhan, China).

2.2 DPPH radical scavenging activity

Based on the method slightly modified from that of LiX et al[20], a mother liquor of 2,2-Diphenyl-1-picrylhydrazyl (DPPH) was prepared with ethanol. Subsequently, various concentrations of PB2 and Trolox (serving as the positive control) were prepared. Then, DPPH was added to the sample to be tested, and the mixture was mixed thoroughly and allowed to rest for 30 minutes. The absorbance was then measured at 517 nm using a microplate reader (Thermo Fisher Scientific Inc., Rockford, USA).

2.3 Enzymes inhibitory activity

2.3.1 The α-amylase activity assay

This test was performed based on the method slightly modified from Bhatnagar A et al[21]. In brief, different concentrations of PB2 and acarbose (serving as the positive control) were prepared. The α-amylase (2 U/mL) was added to each sample, and the mixtures were incubated at 37 ℃ for 10 minutes. Subsequently, 1% starch solution was added to each mixture, followed by incubation again. 3,5-dinitrosalicylic acid (DNS) was added to terminate the reaction, and the mixtures were boiled at 100 ℃ for 10 minutes. The samples were then quickly cooled, and the absorbance was measured at 540 nm.

2.3.2 The α-glucosidase activity assay

This test was performed with slight modifications according to H.F. et al[22]. In brief, different concentrations of PB2 and acarbose were prepared. The α-glucosidase (5 U/mL) was added to samples and incubated at 37 ℃ for 10 minutes. Subsequently, the substrate *p*NPG (3 mM) was added into the pre-incubated mixtures at 37 ℃ for 20 minutes, then 0.1 mol/L Na2CO3 was added to terminate the reaction, and the absorbance was measured at 405 nm.

2.4 Network pharmacology analysis

2.4.1 PB2 and T2DM target prediction

The chemical structure of PB2 was retrieved from the PubChem platform (accessed on March 27, 2024; https://pubchem.ncbi.nlm.nih.gov/), along with its CAS number. The molecular targets of PB2 were sourced from the PharmMapp Server on the same date. Relevant targets were searched using keywords like "type 2 diabetes," "T2DM," and "diabetes type 2" in both the GeneCards (April 1, 2024; http://www.genecards.org/) and OMIM (April 1, 2024; http://www.omim.org/) databases. The retrieved disease targets were then sorted, filtered to exclude duplicates, and limited to human species.

2.4.2 Network construction and PPI analysis

Venn diagrams of the components and disease targets were created using Venny 2.1 (accessed April 10, 2024; https://bioinfogp.cnb.csic.es/tools/venny/index.html/). These intersecting targets were then imported into the STRING database (accessed April 11, 2024; https://string-db.org/) for protein-protein interaction (PPI) analysis, and the results of PPI analysis were visualized using Cytoscape 3.8.2.

2.4.3 GO and KEGG pathway enrichment analysis

Common targets of PB2 and T2DM were imported into the David database (accessed on 16 April 2024; https://david.ncifcrf.gov/) for Gene Ontology (GO) functional annotation and Kyoto Encyclopedia of Genes and Genomes (KEGG) enrichment analysis. A p-value < 0.05 indicates a statistically significant difference. Results were processed with tools from bioinformatics. PPI networks were analyzed using Cytoscape 3.8.2 software to construct a 'PB2-target-pathway' network.

2.5 Cell culture and cell viability

HepG2 cells, obtained from the Cell Bank of the Chinese Academy of Sciences, were cultured in MEM medium supplemented with 1% penicillin-streptomycin and 10% FBS at 37°C in 5% CO_2. Prior to stimulation of the cells with high glucose, two distinct cell groups were pretreated with the Nrf2 inhibitor

ML385 (5 μM) and the PI3K/AKT inhibitor LY294002 (25 μM) for 1 h, respectively, and were designated as the inhibitor groups. Cell viability was evaluated using the CCK-8 kit in HepG2 cells plated in 96-well plates. Subsequently, the medium was replaced with fresh medium containing varying concentrations of GlcN or PB2. After 24 h incubation, the absorbance was measured at 450 nm.

2.6 Establishment of the IR-HepG2 model

The IR-HepG2 model was established following protocols outlined in previous literature[23]. HepG2 cells were cultured in 96-well plates (1×10^5 cells/well). After replacing the medium, each well was supplemented with fresh medium containing varying concentrations of GlcN. Following 24 h incubation, the glucose levels in the supernatants were assayed to determine the optimal GlcN concentration. Subsequently, HepG2 cells were re-cultured, incubated with this optimal GlcN concentration for different durations, and supernatant glucose levels were measured again to ascertain the most suitable incubation time

2.7 Detect glucose consumption, glycogen content, SOD, GSH, CAT, and MDA

After successfully establishing a cell model, we added MET along with various concentrations of PB2, and then incubated the cells for 24 h. Subsequently, we measured cellular glucose consumption, glycogen content, SOD activity, CAT activity, GSH content, and MDA level using the corresponding detection kits according to the manufacturers' instructions.

2.8 Cell fractionation and EMSA

HepG2 cells were treated with or without indicated concentrations of PB2 (20 μM) and GlcN (12 mM) for 24 h. Cells were washed with PBS, collected by centrifugation at 3,000 rpm for 10 min at 4°C, and resuspended in 200 μL pre-chilled cytoplasmic lysis buffer. Homogenization was achieved by gentle pipetting, followed by 5 s vortexing and 15 min ice incubation for plasma membrane lysis. After adding 10 μL stabilizer (cytoplasmic protein reagent B), samples were vortexed for 5 s, incubated on ice for 1 min, vortexed again, and centrifuged at 14,000×g for 5 min at 4°C. Supernatants (cytoplasmic fractions) were collected. Pellets were resuspended in 50 μL nuclear lysis buffer, vortexed for 30 s, and incubated on ice with intermittent vortexing (30 s every 2 min for 30 min) to disrupt nuclear membranes. Nuclear extracts were obtained by centrifugation at 14,000×g for 10 min at 4°C.

A Gelshift™ chemiluminescent electrophoretic mobility shift assay (EMSA) kit was used. A double-stranded DNA probe containing the ARE core sequence (5'-TTTTATGCTGTGTCATGGTT-3') was PAGE-purified and 50-biotinylated via end-labeling. Labeling efficiency was verified by probe mobility. Unlabeled homologous DNA served as a competitor. Nuclear extracts (4 μg) were incubated with biotinylated probe (20 fmol) in binding buffer at RT for 20 min. For competition assays, a 200× molar excess of unlabeled specific probe (4 pmol) was added. Reactions were resolved on 6% native PAGE. Complexes were transferred to nylon membranes, cross-linked under 312 nm UV for 10 min, and detected via chemiluminescence.

2.9 Transfection of small interfering RNA (siRNA)

Predesigned siRNA against human Nrf2 and control scrambled siRNA were purchased from Ambion (Austin, TX, USA). HepG2 cells were plated at a density of 5×10^5 cells per 6cm dish. Cells were transfected with 100 nM siRNA against Nrf2 or 50 nM scrambled duplex by using LipofectAMINE 2000 (Invitrogen). HepG2 cells were exposed to si-Ctrl, scrambled siRNA, or si-Nrf2 for 48 h, and then treated with or without PB2 (20 μM) and GlcN (12 mM) for 24 h and lysed for Western blotting.

2.10 Molecular docking

Molecular docking was conducted based on the results validated *in vitro* to elucidate the interactions between PB2 and the key target proteins AKT, Nrf2, GSK3β, and FoxO1 in alleviating IR. The structure of the small molecular compound was downloaded from PubChem (https://pubchem.ncbi.nlm.nih.gov/). Additionally, the 3D structures of the target proteins AKT (PDB ID: 6HHI), Nrf2 (PDB ID: 3ZGC), GSK3β (PDB ID: 8XN6), and FoxO1 (PDB ID: 3CO6) were obtained from the RCSB PDB website (http://www.rcsb.org/). Prior to docking, the structures were preprocessed using Pymol 2.3.0 software. Subsequently, the receptor and ligands were docked using Autodock Vina 1.2.2 software, and the binding energy was calculated based on the interaction between the protein and small molecule ligands. The results were visualized using Pymol software.

To further explore and comprehensively analyze the relationships between these key target proteins from a different perspective, another molecular docking approach using HADDOCK was employed. For this HADDOCK-based docking, the protein PDB structure files used were the same as those obtained from the RCSB PDB website in the previous Autodock Vina docking procedure. First, we prepared the protein PDB structure files. Then, we preprocessed them using HADDOCK, during which the active and passive sites were defined and the docking parameters were set. Subsequently, we utilized HADDOCK to carry out rigid docking, semiflexible optimization, and all-atom refinement calculations in sequence. After that, analyze the clustering and docking quality of the results. Finally, import the docking models into PyMOL for further visualization and analysis.

2.11 Pull-Down assay

Briefly, PB2 (5 mg) was coupled to CNBr-activated Sepharose 4B beads (75 mg) in a coupling buffer overnight at 4℃. The coupled beads were washed with 5 volumes of coupling buffer and then centrifuged at 110×g for 3 min at 4℃. The precipitate was resuspended in 5 volumes of 0.1M Tris-HCl buffer (pH 8.0) with 2 h rotation at room temperature. After washing three times with 0.1M acetate buffer (pH 4.0) containing 0.5M NaCl, the mixture was further washed with 0.1M Tris-HCl (pH 8.0) buffer containing 0.5M NaCl. The HepG2 cell lysate (500 mg/mL) was incubated at 4℃ overnight with Sepharose 4B beads or PB2-Sepharose-4B coupled beads (100 μL,50% slurry) in reaction buffer (NP-40). The beads were washed five times with washing buffer, and the bound proteins were then eluted and detected by Western blot.

2.12 GST pulldown assay

After fusing the target protein with a GST tag, the target protein and its interacting proteins were purified from cell lysates using the glutathione affinity of GST, followed by identification of interacting proteins via Western Blot. The gene encoding the target protein was inserted into a GST expression vector and transfected into 293T cells or transformed into E. coli BL21 for expression. Cells were then lysed with RIPA lysis buffer (containing protease inhibitors), and GST affinity resin (Glutathione Sepharose 4B) was added, followed by incubation at 4℃ with gentle shaking for 2 hours. After binding with shaking, the resin is washed to remove non-specific proteins. The GST-fusion protein and bound interacting proteins are eluted with glutathione.

2.13 Animals experiment

Thirty specific pathogen-free (SPF) male *db/db* mice (body weight: 20–22 g; age: 5 weeks) were selected and all housed in a controlled environment at the Hunan Provincial Center for Drug Safety Evaluation and Research. The animal production license number is HNSE2025(5)024. The mice were kept under standard conditions of room temperature of 22±2 °C, humidity of 50%±5%, and 12 h light/12 h dark cycle. The concentration of PB2 was set with reference to relevant experimental studies[24][25]. After one week of adaptive feeding, the mice were weighed to record their initial body weight, and then randomly divided into five groups (n=6 each): control group (normal feed), model group, positive control metformin group (MET, 200 mg/kg, oral gavage), PB2 low-dose group (PB2-L, 100 mg/kg, oral gavage), and PB2 high-dose group (PB2-H, 200 mg/kg, oral gavage). The entire experiment lasted for 4 weeks. During the experiment, a calibrated weighing scale and blood glucose meter were used to monitor the mice's body weight and fasting blood glucose (FBG, after 8 hours of fasting) once a week, with blood samples collected via tail vein puncture for FBG measurement

2.14 Biochemical measurement of liver tissue in mice

After orbital venous blood was collected from mice, it was centrifuged at 3000 rpm at 4°C for 10 minutes. The supernatant was collected, which served as the serum sample for analyzing the levels of TG, TC, HDL-C, and LDL-C.

A 0.1 g sample of liver tissue was taken, and 1 mL of PBS containing protease inhibitors was added. The mixture was homogenized on an ice bath using a tissue homogenizer to ensure complete tissue disruption, then transferred to a centrifuge tube and centrifuged at 8000 rpm at 4°C for 10 min. After supernatant collection, CAT activity, SOD activity, MDA level, and GSH content were detected according to the manufacturers' instructions.

2.15 Histopathological analysis

The mouse liver tissues used for pathological section analysis were excised and fixed in 4% formalin at 25°C. After the tissues were embedded in paraffin, 4 μm sections were stained with hematoxylin-eosin (HE) for hepatic pathological evaluation.

2.16 Cell and liver tissue Western blotting

HepG2 cells and liver tissues were washed with PBS, and then lysed with RIPA lysis buffer containing 1% protease inhibitor and 1% phosphatase inhibitor. Liver tissues were homogenized using a tissue grinder. All samples were incubated on ice for 30 min for complete lysis, and then centrifuged at 4°C, 12000 rpm for 10 min. The supernatants were collected for subsequent experiments.Protein concentration was measured using the BCA Protein Assay Kit. Proteins were separated by SDS-PAGE and transferred to PVDF membranes (Amersham Pharmacia Biotech, Little Chalfont, UK). The membranes were blocked and incubated with primary and secondary antibodies. Protein levels were assessed using a Super ECL Plus kit (XinSaiMei，Suzhou, China) by an Image Quant LAS 4000 mini (General Electric Medical System Co., Ltd., Boston, USA). GAPDH served as the housekeeping protein. Protein bands were quantified with ImageJ.

2.17 Statistical analysis

All experimental results are shown as mean ± standard deviation (n≥3). One-way ANOVA was employed to analyze the differences between samples using GraphPad Prism 8.0.2 software (GraphPad Software, San Diego, CA, USA). A *P*-value < 0.05 was regarded as statistically significant.

3. Results

3.1 The effect of PB2 on DPPH radical scavenging capability

Assessing the influence of PB2 on DPPH radical scavenging capability is crucial for understanding its antioxidant properties and exploring its potential health benefits. Figure 1A shows the structure of PB2, which is a dimer of two flavonoids, specifically catechin or epicatechin. As shown in Figure 1B, both PB2 and trolox exhibited radical scavenging activity on DPPH in a concentration-dependent pattern. The half-maximal inhibitory concentration (IC_{50}) value of PB2 was 73.70 μM, which was lower than that of trolox (IC_{50}=275.1 μM), suggesting that the antioxidant activity of PB2 is higher than that of trolox.

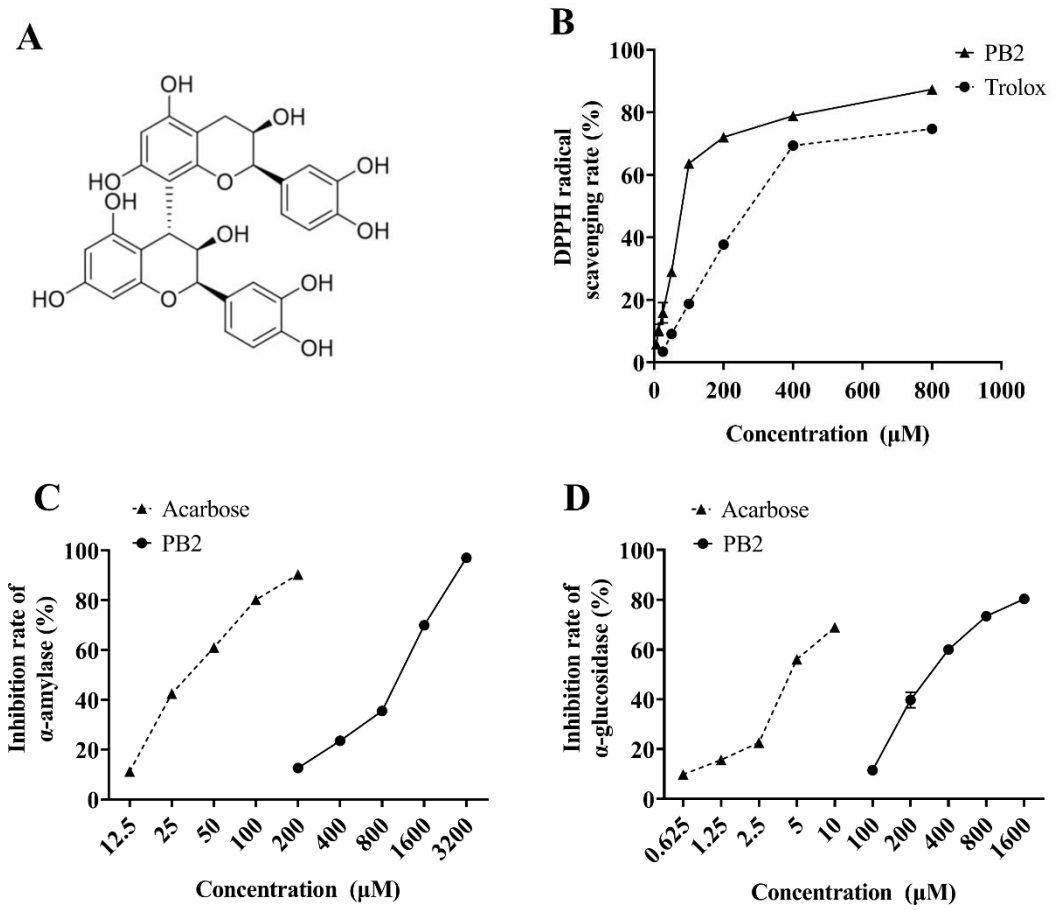

Figure 1. The DPPH antioxidant activity and digestive enzyme inhibitory property of PB2 *in vitro*. (A) The chemical structure of PB2. (B) PB2 and Trolox scavenge DPPH free radicals in a dose-dependent manner. (C) PB2 inhibits the activity of α-amylase vs. acarbose. (D) PB2 inhibits the activity of α-glucosidase vs. acarbose.

3.2 The inhibitory effect of PB2 on the activity of digestive enzymes

Inhibiting α-amylase and α-glucosidase activities indicates potential to delay carbohydrate hydrolysis and attenuate postprandial hyperglycemia. This glucose regulatory effect may synergistically enhance insulin sensitivity by reducing prolonged exposure to hyperglycemic spikes. As shown in Figure 1C, both PB2 and acarbose exhibited inhibitory activities on α-amylase. The IC_{50} value of PB2 was 951.3 μM, which was higher than that of acarbose (IC_{50}=36.3 μM). Similarly, as shown in Figure 1D, both PB2 and acarbose exhibited inhibitory activities on α-glucosidase. The IC_{50} value of PB2 was 331.4 μM, which was higher than that of acarbose (IC_{50}=4.9 μM). The above results indicated that the inhibitory activity of PB2 on α-amylase and α-glucosidase is less effective than that of acarbose. This suggests that the hypoglycemic effect of PB2 is not primarily dependent on the inhibition of digestive enzyme activity. Consistent with the prediction of PI3K/AKT pathway enrichment by network pharmacology, further investigation into the regulatory mechanisms of PB2 on glucose metabolism signaling pathways at the cellular level is warranted.

3.3 Network pharmacology analysis

The 286 targets of PB2 were obtained through screening the PharmMapp Server database. Additionally, the 2372 IR-related targets were sourced from OMIM, GeneCards, and Drugbank databases. As depicted in Figure 2A, the online software Venny2.1 was utilized to identify common targets between

drug action and disease-related targets, ultimately screening out 127 drug-disease common targets. As shown in Figure 2B, the 127 common targets imported into the String database to reveal protein-protein interactions, resulted in a PPI network with 126 nodes and 1,581 edges. This network was then imported into Cytoscape 3.8.2 for further analysis. By eliminating low-correlation dispersion points, a refined PPI network (Figure 2C), was obtained based on intermediate and degree values, consisting of 21 nodes and 223 edges. Node sizes in this network are scaled according to their degree values, with color gradients indicating spacing. Circular nodes signify targets, where larger and darker nodes indicate stronger associations with other proteins in the network, suggesting greater the possibility of functional significance. CASP3, MMP9, and IGF1 indicate strong protein-protein interactions and numerous targets associated with them, which are also considered core targets of PB2 for IR. Notably, AKT and GSK3β, which were studied in this experiment, were also included.

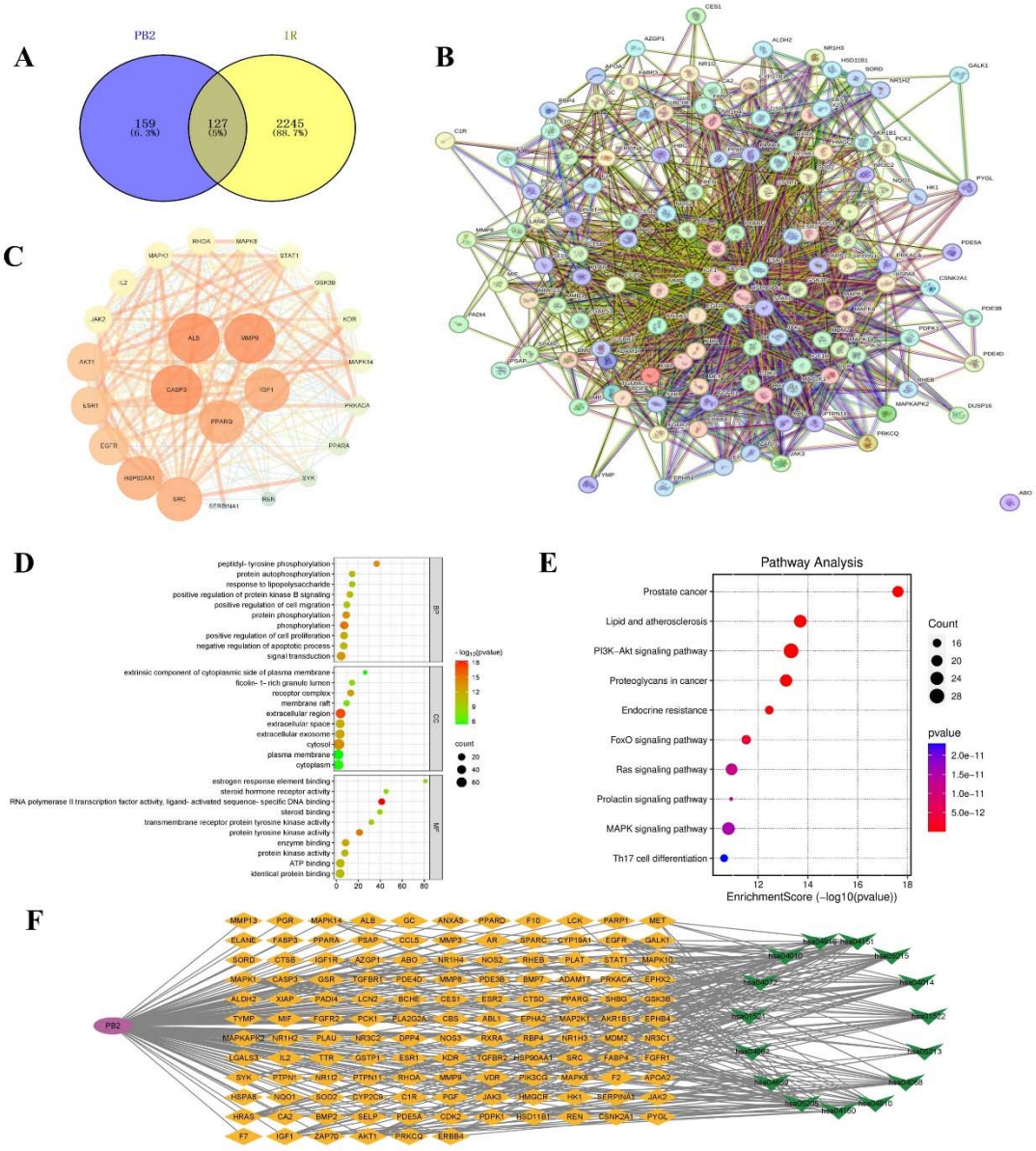

Figure 2. Network pharmacology, along with GO and KEGG enrichment analysis. (A) Venn diagram of targets of PB2 and IR. (B) PPI network diagram of PB2-related IR. (C) Information network of protein interaction. (D) GO enrichment analysis. (E) KEGG pathway enrichment analysis. (F) Network diagram of "PB2-target-pathway".

KEGG and GO databases are prevalent in bioinformatics and are often utilized for network pharmacological mechanism predictions. Thus, we explored the potential mechanism of PB2 in mitigating IR through enrichment analysis. Our GO analysis, which focused on 127 common target genes for PB2 and IR using the DAVID database, encompassed biological processes (BP), cellular components (CC), and molecular functions (MF). As illustrated in Figure 2D, the top 10 items in each category were ranked based on count values, with a significance threshold of p-value <0.05. BP mainly includes peptidyl-tyrosine phosphorylation, protein autophosphorylation, response to lipopolysaccharide, positive regulation of protein kinase B signaling, positive regulation of cell migration, protein phosphorylation, phosphorylation, positive regulation of cell proliferation, negative regulation of cell apoptosis process, and signaling transduction. CC mainly includes extrinsic component of cytoplasmic side of plasma membrane, ficolin-1-rich granule lumen, receptor complex, membrane raft, extracellular region, extracellular space, extracellular exosome, cytosol, plasma membrane, and cytoplasm. MF mainly includes estrogen response element binding, steroid hormone receptor activity, RNA polymerase II transcription factor activity, ligand-activated sequence-specific DNA binding, steroid binding, transmembrane receptor protein tyrosine kinase activity, protein tyrosine kinase activity, enzyme binding, protein kinase activity, ATP binding, and identical protein binding. As shown in Figure 2E, KEGG pathways were significantly enriched by PB2 treatment, and the results found that PB2 was mainly involved in prostate cancer, lipid and atherosclerosis, PI3K/AKT signaling pathway, endocrine resistance, FoxO signaling pathway, Ras signaling pathway, MPAK signaling pathway and Th17 signaling pathway.

Next, the construction and analysis of the "component-target-pathway" network was conducted. As shown in Figure 2F, chemical components are shown in purple, targets in yellow, and the top 15 significant pathways in green, respectively, and the major protein targets of PB2 intervention in T2DM include PI3K, AKT1, GSK3β, MAPK1, JAK2, PCK1, IGF1, and IL2. Meanwhile, the main signaling pathways regulated by PB2 in T2DM include insulin signaling pathway (hsa04910), PI3K-AKT signaling pathway (hsa04151), FoxO signaling pathway (hsa04068), MAPK signaling pathway (hsa04010), Th17 signaling pathway (hsa04659), and endocrine resistance (hsa01522), and respective genes associated with the above signaling pathways are shown in Table 1.

Table 1. Genes associated with signaling pathways regulated by PB2 treatment

KEGG ID	Pathways	Genes	*P*-Value	Fold Enrichment
hsa04151	PI3K-AKT signaling pathway	GSK3β, PIK3CG, AKT1, MAPK1, JAK2, PCK1, IGF1	8.81×10^{-14}	5.844
hsa04910	Insulin signaling pathway	GSK3β, PYGL, HK1, AKT1, MAPK1, PCK1	2.74×10^{-9}	8.213
hsa04068	FoxO signaling pathway	MAP2K1, IGF1, SOD2, CDK2, AKT1	1.20×10^{-11}	9.730
hsa05215	Prostate cancer	GSK3β, MAP2K1, IGF1R, AR, CDK2, MDM2, AKT1	1.35×10^{-17}	15.4195
hsa04010	MAPK signaling pathway	HSPA8, MAP2K1, MAPK8, MAPK2, KDR, AKT1	3.42×10^{-11}	5.792
hsa05205	Proteoglycans in cancer	MAP2K1, PDPK1, IGF1, MAPK14, MDM2, AKT1	1.43×10^{-13}	8.148

KEGG ID	Pathways	Genes	*P*-Value	Fold Enrichment
hsa01522	Endocrine resistance	MAP2K1, PDPK1, IGF1, MAPK14, MDM2, AKT1	2.01×10^{-12}	12.211
hsa04014	Ras signaling pathway	MAP2K1, IGF1, PGF, IGF1R, AKT1	2.56×10^{-11}	6.667
hsa04659	Th17 cell differentiation	HSP90AA1, STAT1, IL2, MAPK8, MAPK1, JAK2	1.01×10^{-10}	10.494
hsa05213	Endometrial cancer	GSK3β, PDPK1, MAPK1, AKT1, EGFR	1.15×10^{-4}	8.964

3.4 IR-HepG2 model construction and the effect of PB2 on cell viability and glucose consumption

To establish an optimal IR-HepG2 model, we first determined the best concentration and induction time for GlcN. Initially, we assessed how various GlcN concentrations impacted HepG2 cell viability. Figure 3A-B showed that, after 24 h of induction with GlcN concentrations ranging from 0 to 30 mM, concentrations from 0 to 12 mM had no inhibitory impact on cell viability compared to the control group ($p>0.05$). However, at 18 mM, GlcN showed obvious cytotoxicity and concentrations from 24 to 30 mM exhibited significant toxicity ($p<0.05$). Screening for the optimal GlcN concentration showed that glucose consumption decreased as the concentration increased from 6 to 30 mM. Notably, 12 mM GlcN showed a more pronounced effect ($p<0.01$), and this concentration had no impact on cell viability ($p>0.05$). The difference was statistically notable when compared to the control group. Therefore, 12 mM was chosen as the optimal induction concentration. Further optimal induction time was investigated in HepG2 cells. As illustrated in Figure 3C, the model group exhibited significantly reduced glucose consumption compared to the control group. The most significant difference in glucose consumption between the two groups was observed at 24 h of induction, with the model group showing a 2.6 mmol/L decrease compared to the control group ($p<0.001$). Consequently, the optimal concentration and induction time for the cell model were determined to be 12 mM and 24 h, respectively.

After the cell model was successfully established, we evaluated the impact of various PB2 concentrations (10~320 μM) on HepG2 cell viability. Figure 3D demonstrated that PB2 at 320 μM exhibited notable cytotoxicity ($p<0.001$), whereas other concentrations had no significant effect on cell viability and were considered safe ($p>0.05$). Consequently, the low (20 μM) and high (40 μM) doses of PB2 were selected for subsequent investigations. We then investigated the influence of PB2 on glucose consumption and content. As shown in Figure 3E-F, the model group displayed significantly reduced glucose consumption and uptake compared to the control group ($p<0.01$). However, PB2 treatment significantly increased both glucose consumption and uptake ($p<0.05$). These findings indicated that PB2 could alleviate glucose metabolism disorders induced by high glucose treatment and decrease IR in IR-HepG2 cells.

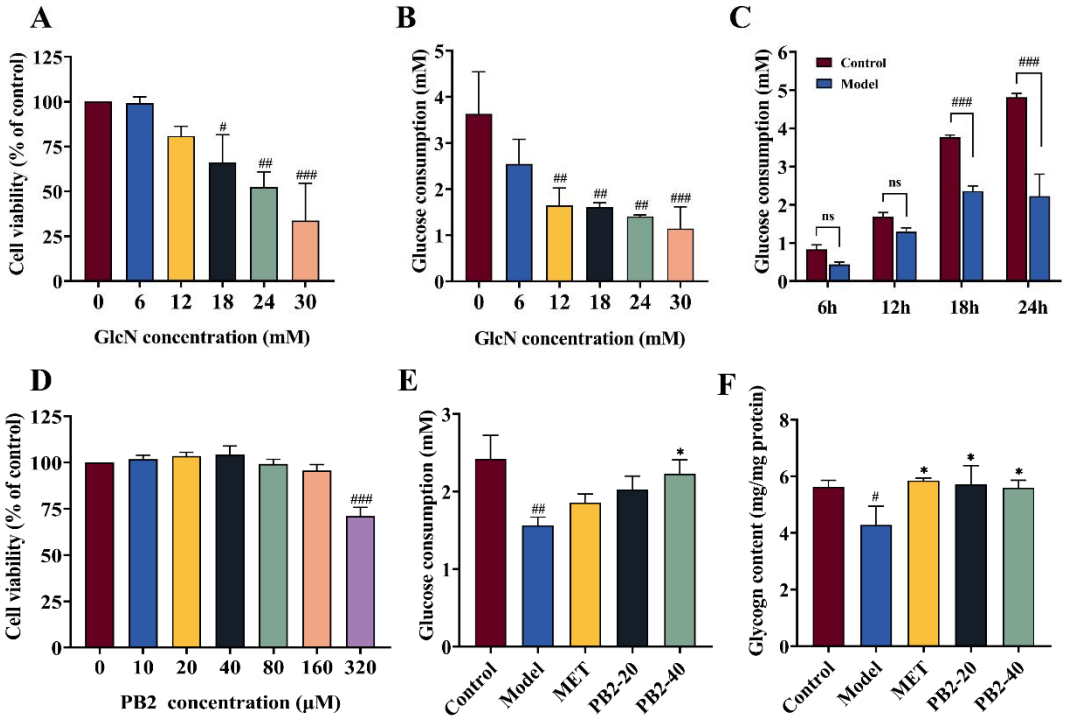

Figure 3. The establishment of insulin resistance cell model (IR-HepG2). (A) The cell viability of HepG2 cells treated by various concentrations of GlcN for 24 h. (B) The dose-response relationship of GlcN on glucose consumption in HepG2 cells, and (C) the time course of glucose consumption in HepG2 cells treated with GlcN. (D) The cell viability of HepG2 cells treated with different concentrations of PB2 for 24 h. (E) The effect of different doses of PB2 on glucose consumption in IR-HepG2 cells. (F) The glycogen content assay in the IR-HepG2 cells. Data are expressed as mean ± SD (n≥3), $^{\#}P<0.05$, $^{\#\#}P<0.01$, $^{\#\#\#}P<0.001$ vs. control group; $^{*}P<0.05$ vs. model group.

3.5 PB2 improves IR by glucose metabolism regulation via IRS1/PI3K/AKT signaling pathway

Insulin signaling is a major pathway controlling glucose metabolism in liver tissue, and inhibition of some signaling pathways leads to a decreased insulin sensitivity, which results in IR[26]. To investigate the impact of PB2 on improving high glucose induced IR in HepG2 cells, the expressions of IRS1 and AKT were detected. As shown in Figure 4A-C, compared with the control group, the expressions of p-IRS1/IRS1 and p-AKT/AKT were significantly reduced in the model group ($p<0.05$, $p<0.01$), and treatment with PB2 and MET significantly promoted the expressions of p-IRS1/IRS1 and p-AKT/AKT ($p<0.05$, $p<0.01$). Furthermore, GLUT4 has been shown to be a key target for glucose transport to various organs[27]. As shown in Figure 4D, the expression of GLUT4 was significantly suppressed in model cells compared with the control group ($p<0.001$); however, MET and PB2 treatment significantly promoted GLUT4 expression ($p<0.05$, $p<0.01$). These results indicated that PB2 could increase the insulin utilization and alleviate IR in HepG2 cells via activation of IRS1/PI3K/AKT signaling pathway.

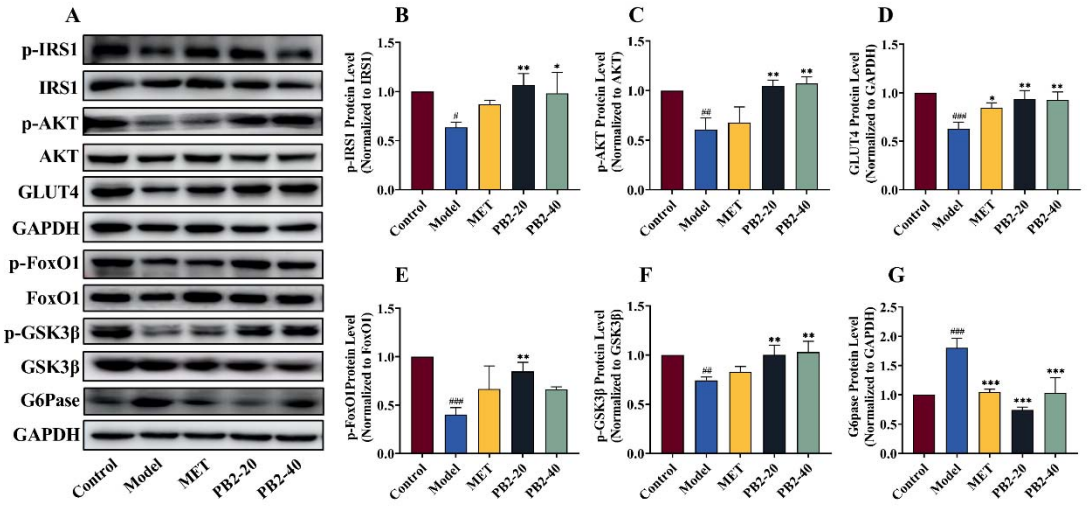

Figure 4. The effect of PB2 in regulating glucose metabolism to improve IR in IR-HepG2 cells. (A) Combination on protein levels. The effect of PB2 on the expressions of proteins (B) p-IRS1, (C) p-AKT, (D) GLUT4, (E) p-FoxO1, (F) p-GSK3β, and (G) G6pase. Data are expressed as mean ± SD (n≥3), $^{\#}P$ <0.05, $^{\#\#}P$ <0.01, $^{\#\#\#}P$ <0.001 vs. control group; $^{*}P$ <0.05, $^{**}P$ <0.01, $^{***}P$ <0.001 vs. model group.

Western Blot was performed to continue detecting the expression levels of FoxO1 and GSK3β in IR-HepG2 cells, which are associated with gluconeogenesis and glycogen synthesis, respectively. As shown in Figure 4E-F, compared with the control group, the expressions of p-FoxO1 and p-GSK3β in the model group were significantly reduced (p＜0.01, p＜0.001), and treatment with PB2 and MET both significantly increased their expression levels (p＜0.01). Furthermore, G6pase is known to be a key enzyme in gluconeogenesis. As shown in Figure 4G, high glucose stimulation significantly increased G6pase expression compared to control (p＜0.001), whereas PB2 and MET both significantly reduced G6pase expression (p＜0.001). The above results indicated that PB2 treatment could improve IR by inhibiting gluconeogenesis and promoting glycogen synthesis through regulation of IRS1/PI3K/AKT pathway.

3.6 PB2 enhances antioxidant activity by the induction of Nrf2/HO-1 pathway

To investigate the protective effect of PB2 in mitigating oxidative damage induced by hyperglycemia, we measured GSH content, SOD activity, CAT activity and MDA level in IR-HepG2 cells using specific kits. As illustrated in Figure 5A-C, the model group exhibited significantly decreased GSH content, SOD and CAT activity compared to the control group (p＜0.05, p＜0.01). However, PB2 treatment significantly increased these activities in IR-HepG2 cells, aligning with the observations seen with MET (p＜0.05, p＜0.01). Furthermore, we evaluated MDA level, a marker of oxidative stress, as shown in Figure 5D. The model group had significantly elevated MDA level compared to the control group (p＜0.01). Notably, treatment with PB2 and MET significantly reduced MDA level (p＜0.01).

These results indicated that PB2 protected IR-HepG2 cells from oxidative damage. To further explore whether the antioxidant effect of PB2 was linked to the activation of the Nrf2/HO-1 signaling pathway, we conducted analysis to assess the expressions of Nrf2, HO-1, and NQO1. As depicted in Figure 5E-H, the model group showed significantly decreased expressions of these proteins compared to the control group (p＜0.01, p＜0.001,). MET and PB2 treatment notably increased their expressions (p＜0.05, p＜0.01). These

findings imply that PB2 restores the redox balance in HepG2 cells by activating the Nrf2/HO-1 signaling pathway, including enhancing the expressions of key proteins and antioxidant enzymes.

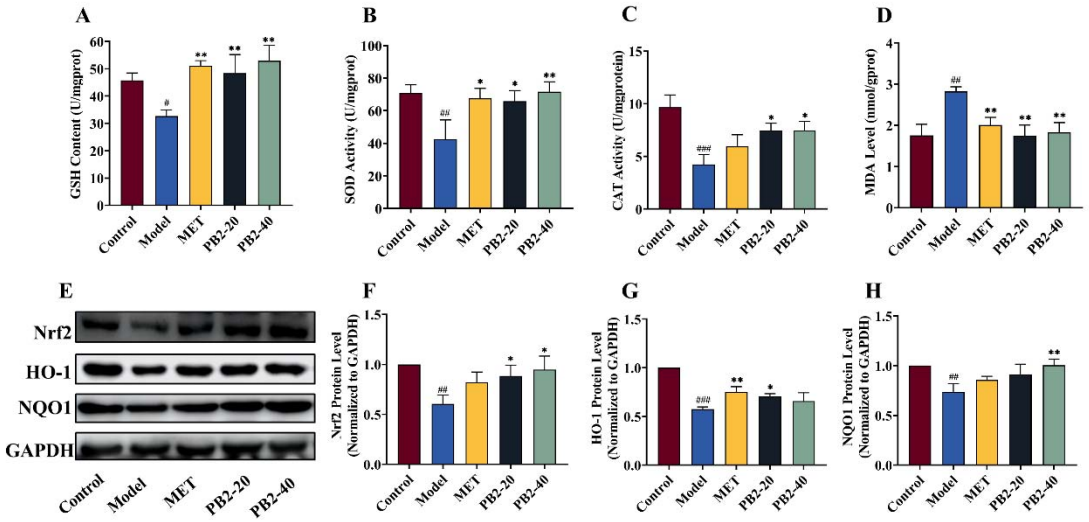

Figure 5. The effect of PB2 on the antioxidant capacity in IR-HepG2 cells. (A) GSH content. (B) SOD activity. (C) CAT activity. (D) MDA level. (E) Combination on protein levels. The effect of PB2 on the expressions of proteins (F) Nrf2, (G) HO-1, and (H) NQO1. Data are expressed as mean ± SD (n≥3), $^{\#}P$ <0.05, $^{\#\#}P$ <0.01, $^{\#\#\#}P$ <0.001 vs. control group; $^{*}P$ <0.05, $^{**}P$ <0.01, $^{***}P$ <0.001 vs. model group.

3.7 PB2 increases protein stability and nuclear translocation of Nrf2 to enhance ARE binding ability

To block protein synthesis, HepG2 cells were pretreated with the combination of the protein synthesis inhibitor cycloheximide (CHX, 5 μg/ml) and PB2 (20 μM). As shown in Figure 6A-B, we calculated the half-life ($t_{1/2}$) from protein decay experiments. Treatment with PB2 extended the half-life ($t_{1/2}$) of Nrf2 protein from 40.03 to 70.79 min. The result indicated that PB2 increased Nrf2 protein expression by inhibiting the turnover of Nrf2 at the posttranslational level.

The nuclear translocation of Nrf2 and its ARE binding capacity are essential primary actions during Nrf2-mediated ARE activation. To further clarify the effects of PB2 on these actions, we first examined the localization of Nrf2 in the cells treated with or without PB2 (20-40 μM) and GlcN (12 mM) for 24 h. As shown in Figure 6C-D, PB2 promoted the nuclear translocation of Nrf2, as evidenced by increased nuclear Nrf2 levels (p<0.01). The integrity of the cytosolic and nuclear fractions was confirmed with cytosolic GAPDH and nuclear lamin B proteins.

To demonstrate whether Nrf2 accumulated in the nuclear by PB2 actually binds to the ARE, we examined the ARE-binding complexes by chemiluminescent EMSA with biotin-labeled human ARE oligonucleotides. Competitive experiments demonstrated that cotreated with 4 pmol of unlabeled human ARE oligonucleotides substantially blocked the formation of this DNA-protein complex (Figure 6E, lane 2). Notably, PB2 enhanced ARE-binding complexes in dose-dependently manner (Figure 6E, lanes 3-4). These results indicated that PB2 induced Nrf2-mediated ARE activation through increasing the nuclear accumulation of Nrf2 and sequential binding of Nrf2 to ARE.

Moreover, to confirm whether the upregulation of Nrf2 was a pivotal factor by PB2, we transfected siRNA molecules specifically targeting Nrf2 into HepG2 cells. As illustrated in Figure 6F-G, the Nrf2

siRNA reduced the basal Nrf2 and NQO1 (lane 5 compared to lane 1) ($p<0.05$). The levels of Nrf2 and NQO1 proteins that were induced by PB2 were decreased (lane 6 compared to lane 2) ($p<0.001$). In contrast, when compared to the control group, the scrambled siRNA did not produce any such inhibitory effect ($p>0.05$). These findings distinctly revealed that the disruption of Nrf2 expression can effectively inhibit the elevation of related proteins that is brought about by PB2.

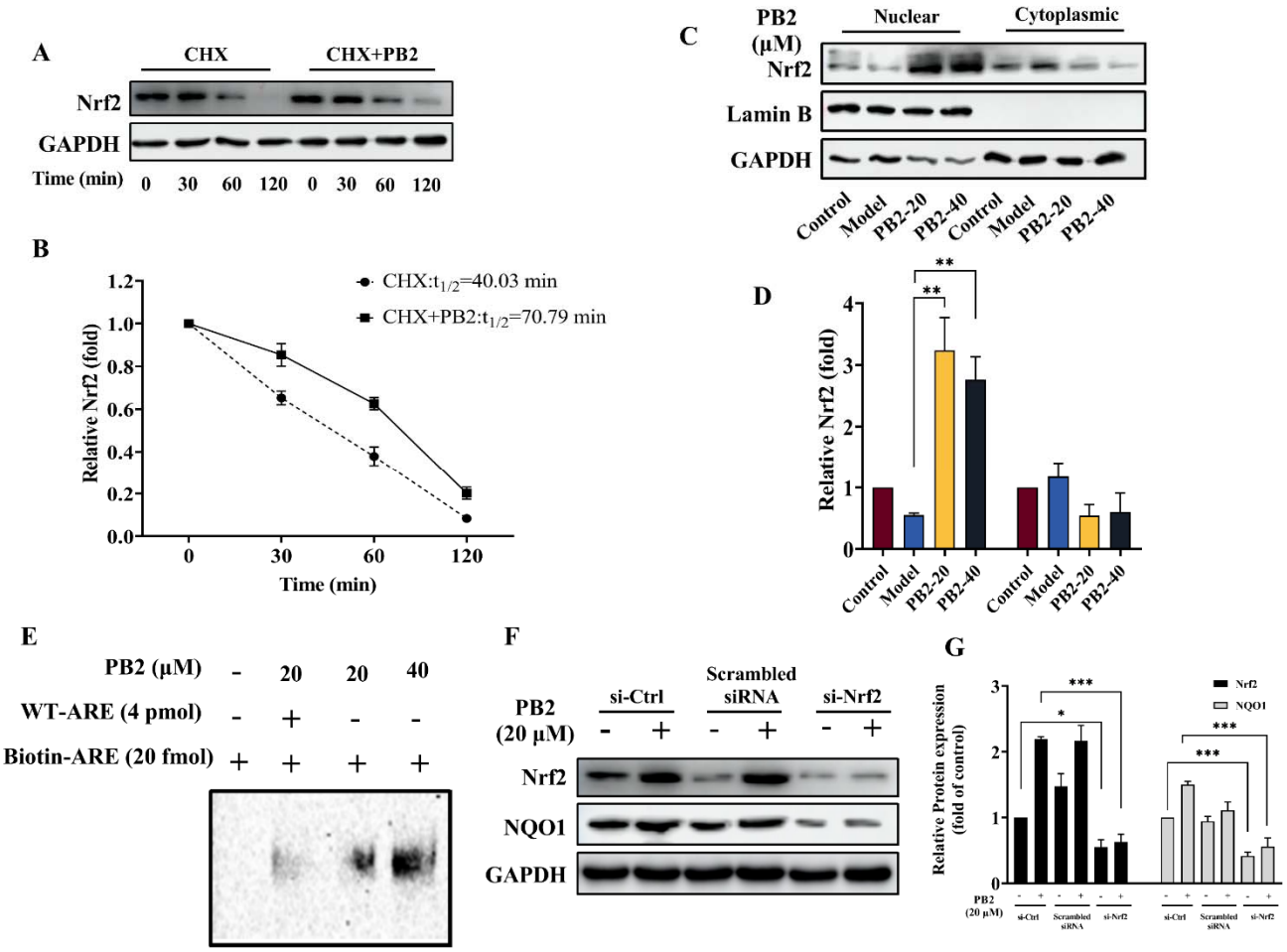

Figure 6. PB2 increases protein stability and nuclear translocation of Nrf2 to enhance ARE binding ability. (A-B) PB2 stabilizes Nrf2 protein. (C-D) PB2 promotes Nrf2 nuclear accumulation. (E) PB2 enhances the ARE binding activity. (F-G) siRNA of Nrf2 interrupts PB2-stimulated Nrf2 and NQO1 expressions. Data are expressed as mean ± SD (n≥3), $^{**}P<0.01$, $^{***}P<0.001$.

3.8 The effect of inhibitors on PI3K/AKT-Nrf2-GSK3β signaling pathway

To explore the relationship between PI3K/AKT and Nrf2 signals, the regulatory relationship between PI3K/AKT and Nrf2 signaling pathways was investigated in IR-HepG2 cells using pathway-specific inhibitors. As illustrated in Figure 7A, ML385 and LY294002 were found to significantly inhibit the expression of Nrf2 and AKT, respectively. As shown in Figure 7B-E, pharmacological inhibition of PI3K/AKT signaling with LY294002 significantly reduced both p-AKT and Nrf2 protein expression levels ($p<0.01$, $p<0.001$). This suppression of Nrf2 may stem from a reciprocal regulatory mechanism between PI3K/AKT signaling and Nrf2, potentially mediated through AKT-mediated phosphorylation that inhibits FoxO1 nuclear translocation, thereby indirectly attenuating Nrf2 target gene expression. Notably, Nrf2 inhibition via ML385 effectively blocked PB2-induced Nrf2 activation while causing only marginal

reduction in p-AKT expression, without completely reversing PB2's stimulatory effects. These findings suggest partial cross-regulation between Nrf2 and PI3K/AKT pathways, with PI3K/AKT likely positioned upstream of Nrf2 signaling. Comparative analysis with PB2-H treated group revealed significant downregulation in Nrf2 expression, p-AKT/AKT ratio, and p-GSK3β/GSK3β ratio following either inhibitor treatment, demonstrating that both pathways serve as critical nodes for PB2-mediated biological effects.

Collectively, the data establish an interdependent regulatory relationship where Nrf2 appears partially regulated by PI3K/AKT signaling. This coordinated regulation of both pathways enhances glucose utilization capacity such as stimulation of p-GSK3β, thereby contributing to the amelioration of IR. The observed cross-talk mechanism provides mechanistic insights into potential therapeutic strategies for metabolic disorders involving IR pathogenesis.

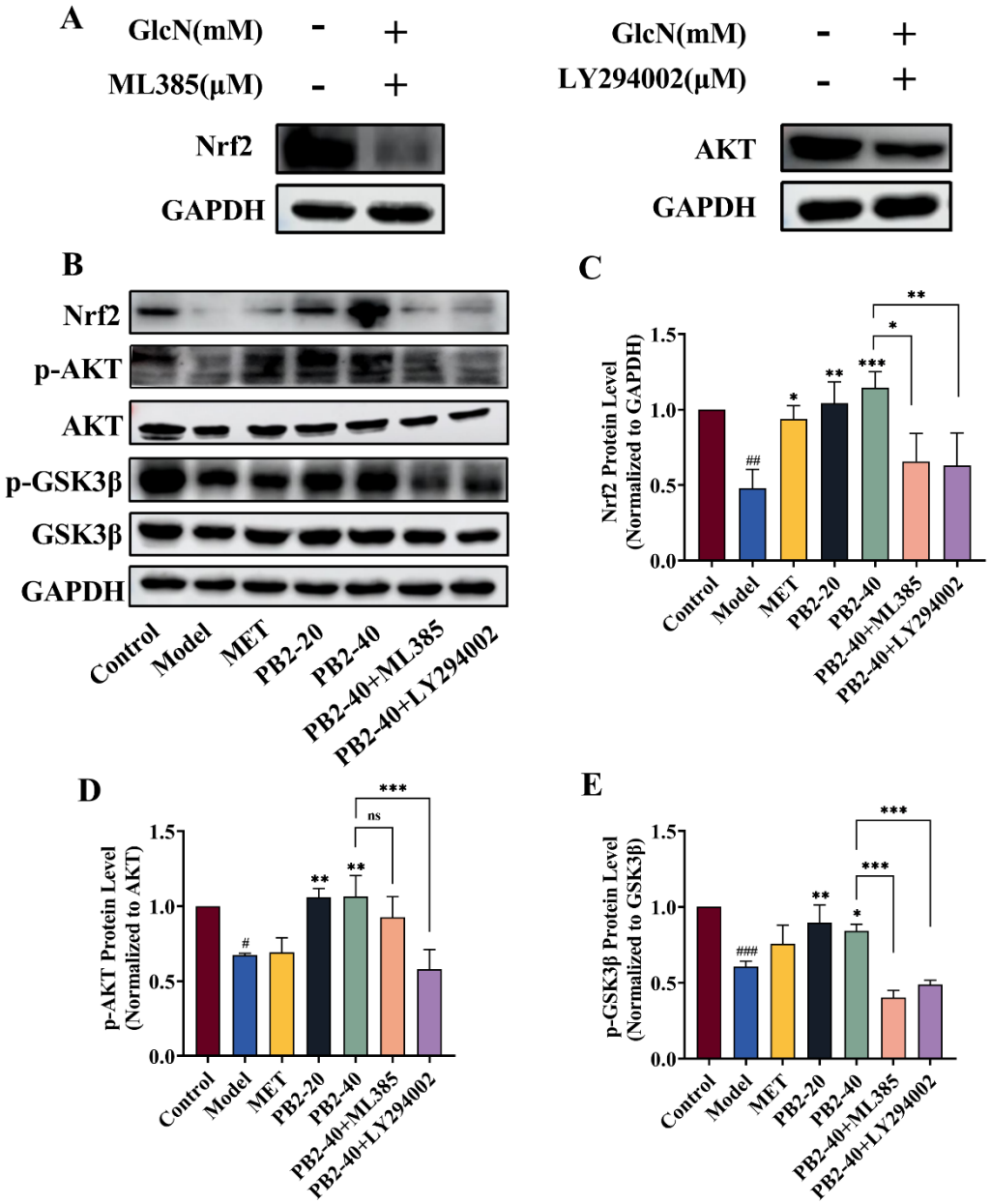

Figure 7. The effect of inhibitors on the Nrf2, AKT, and GSK3β signaling pathways. (A) The expression levels of Nrf2 and AKT alone after treatment with ML385 and LY294002, respectively. (B) Combination on protein levels. The effect of PB2 on the expressions of proteins (C) Nrf2, (D) p-AKT/AKT, and (E) p-GSK3β/GSK3β. Data are expressed as mean ± SD (n≥3), $^{\#}P$ <0.05, $^{\#\#}P$ <0.01, $^{\#\#\#}P$ <0.001 vs. control group; $^{*}P$ <0.05, $^{**}P$ <0.01, $^{***}P$ <0.001 vs. model group.

3.9 Molecular docking and direct binding verification of PB2-Nrf2 and Nrf2-GSK3β

Molecular docking was performed to investigate how PB2 regulates Nrf2 and IR-related proteins. As illustrated in Table 2 and Figure 8A-D, PB2 had significant binding activity with key targets such as AKT, Nrf2, GSK3β, and FoxO1, indicating a strong interaction between PB2 and these targets. Among them, GSK3β has the highest affinity with PB2, which is −9.7 kcal/mol, and the binding sites are GLU-97, LYS-94, LYS-292, ARG-96, GLN-295 and PHE-293. AKT has an affinity of −9.3 kcal/mol, and the binding sites are ARG-48, ARG-328, GLY-394, ALA-329 and ASP-325. Nrf2 has an affinity of −8.4 kcal/mol, and binding sites are ASP-389, ARG-380, ARG-415, GLY-433 and ASN-387. FoxO1 has the lowest affinity, with a binding energy of −7.1 kcal/mol, and its binding sites include ALA-159, TRP-209, TYR-165, and ASN-216. The above results indicated that PB2 may exert its IR improving ability via regulation of PI3K/AKT-Nrf2-GSK3β signaling, more than regulation of FoxO1 signaling pathway. Next, further Pull-Down assay was performed to verify the direct binding of PB2 to Nrf2 and other key targets. As shown in Figure 8E, compared to the cell lysate control, Nrf2 was detected in the complex of PB2-Sepharose 4B beads-proteins, while it was slightly detected in Sepharose 4B beads alone. The data showed that PB2 directly bound to Nrf2, while binding of PB2 to AKT and GSK3β was not detected in this assay (data not shown). This discrepancy between molecular docking and Pull-Down results may be due to the lower binding affinity of PB2 to AKT/GSK3β compared to Nrf2, which falls below the detection limit of the Pull-Down assay.

Table 2. Molecular docking binding of PB2 to key targets

Composition	Protein	PDB ID	Binding Affinity (kcal/mol)
PB2	AKT	6HHI	-9.3
	Nrf2	3ZGC	-8.4
	GSK3β	8XN6	-9.7
	FoxO1	3CO6	-7.1

Moreover, further Pull-Down assay by using GST/Flag system with input target protein was performed to find the direct proof between Nrf2 to IR-related biomarkers. As shown in Figure 8F, In HADDOCK docking analysis, a Z-score<-1.5 for the GSK3β-Nrf2 complex model indicated energy significantly superior to random docking models served as the benchmark for preliminary screening of plausible molecular interaction conformations. As shown in Figure 8G of input lane, GST-GSK3β fusion protein expression vector was first constructed and co-expressed with Flag-Nrf2 in host cells. GST-GSK3β fusion proteins were specifically captured using glutathione-agarose resin, and a negative control group was established using an empty vector system in which GST-β-galactosidase (GST-β-gal) was expressed. As shown in Figure 8G of Pull-Down Lane, the GST-GSK3β eluted fraction from the experimental group exhibited specific detection of the Flag-Nrf2 signal, indicating successful capture of Nrf2 by GSK3β. This indicates that the PI3K/AKT signaling pathway inhibits GSK3β activity through phosphorylation, thereby promoting the binding of GSK3β to Nrf2. In contrast, no Flag-Nrf2 signal was detected in the GST-β-gal eluate from

the negative control group. These findings confirm that GSK3β specifically binds to Nrf2 in *in vitro* model, providing molecular evidence for a direct physical interaction between these two proteins.

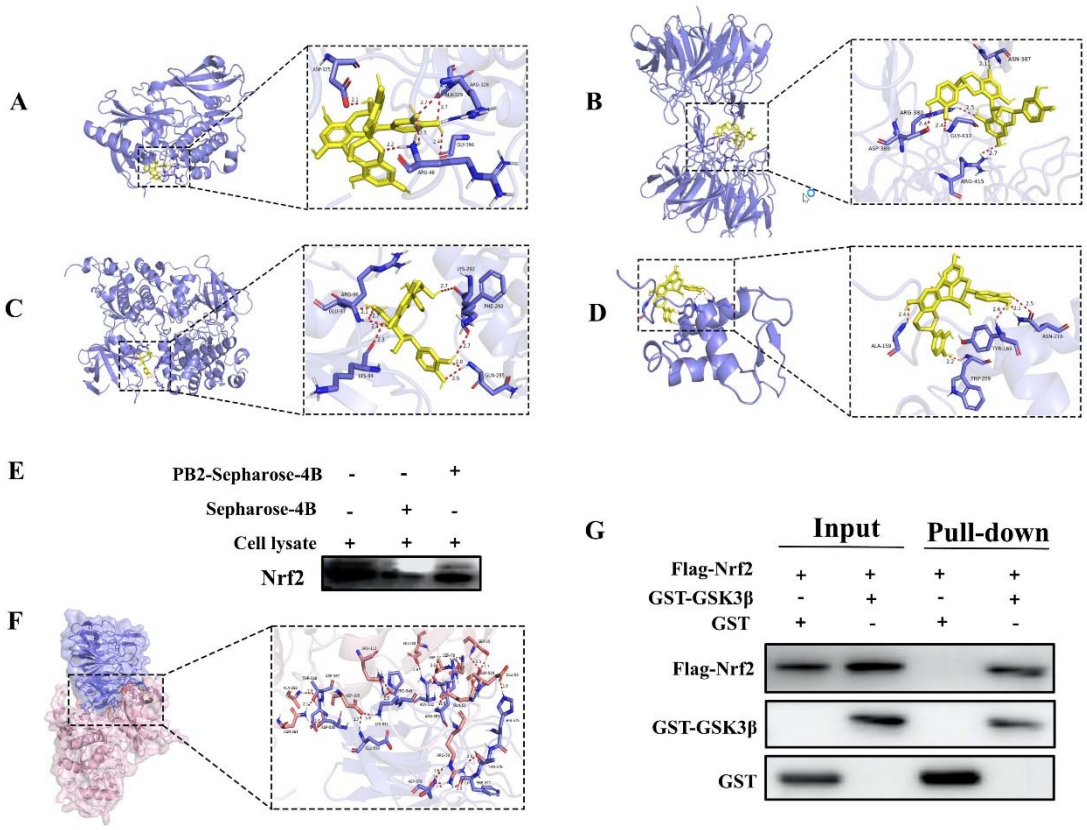

Figure 8. The molecular docking results between PB2 and Nrf2 or IR-related biomarkers, and direct binding proof. The results include global diagrams and details of PB2 docking with: (A) AKT, (B) Nrf2, (C) GSK3β, and (D) FoxO1. (E) Binding abilities of PB2 to Nrf2. (F) The molecular docking results between Nrf2 and GSK3β. (G) GST pull-down assay demonstrates the binding of GST-GSK3β to Nrf2 protein.

3.10 The effect of PB2 on physicochemical indicators and liver injury in db/db mice

To verify the efficiency of PB2 in *in vivo* level, animal experiment by using *db/db* mice was performed. As shown in Figure 9A, there was no significant change in body weight of control group ($p>0.05$), while the weights of other groups were significantly higher than that of the control group. Therefore, these results showed that PB2 had no influence on the body weight of mice. As shown in Figure 9B, MET and PB2 treatments decreased the FBG levels of mice compared with the model group, which is closer to that of the control group, indicating that PB2 reduced the FBG level of *db/db* mice. Moreover, Figure 9C-F showed that the serum levels of TC, TG, and LDL-C in the model group were significantly increased ($p<0.001$), while HDL-C was significantly decreased ($p<0.001$). After MET and PB2 treatment, TC, TG, and LDL-C in *db/db* mice were significantly reduced ($p<0.001$), while HDL-C was significantly increased ($p<0.01$). The above results indicated that PB2 improved the blood lipid and glucose levels in *db/db* mice.

Furthermore, ALT and AST were detected as markers of hepatic steatosis. As shown in Figure 9G-H, compared with the control group, the levels of AST and ALT in the model group were considerably increased ($p<0.001$). After the feeding of PB2, the levels of ALT and AST were considerably decreased, respectively ($p<0.01$, $p<0.001$). Finally, in order to investigate whether PB2 can alleviate liver injury, H&E

staining was performed. As shown in Figure 9I, the liver lobules in the control group were clear, and tissue structure was normal with a complete morphology, while in the model group, the liver cells were massively necrotic, and the cytoplasm was filled with circular lipid droplets of varying sizes. After treatment with MET and PB2, the numbers of vacuoles were significantly reduced, the accumulation of lipid droplets was less and the morphology of liver cells returned to a relatively normal state. These results revealed that PB2 intervention protected liver tissue from IR induced damage.

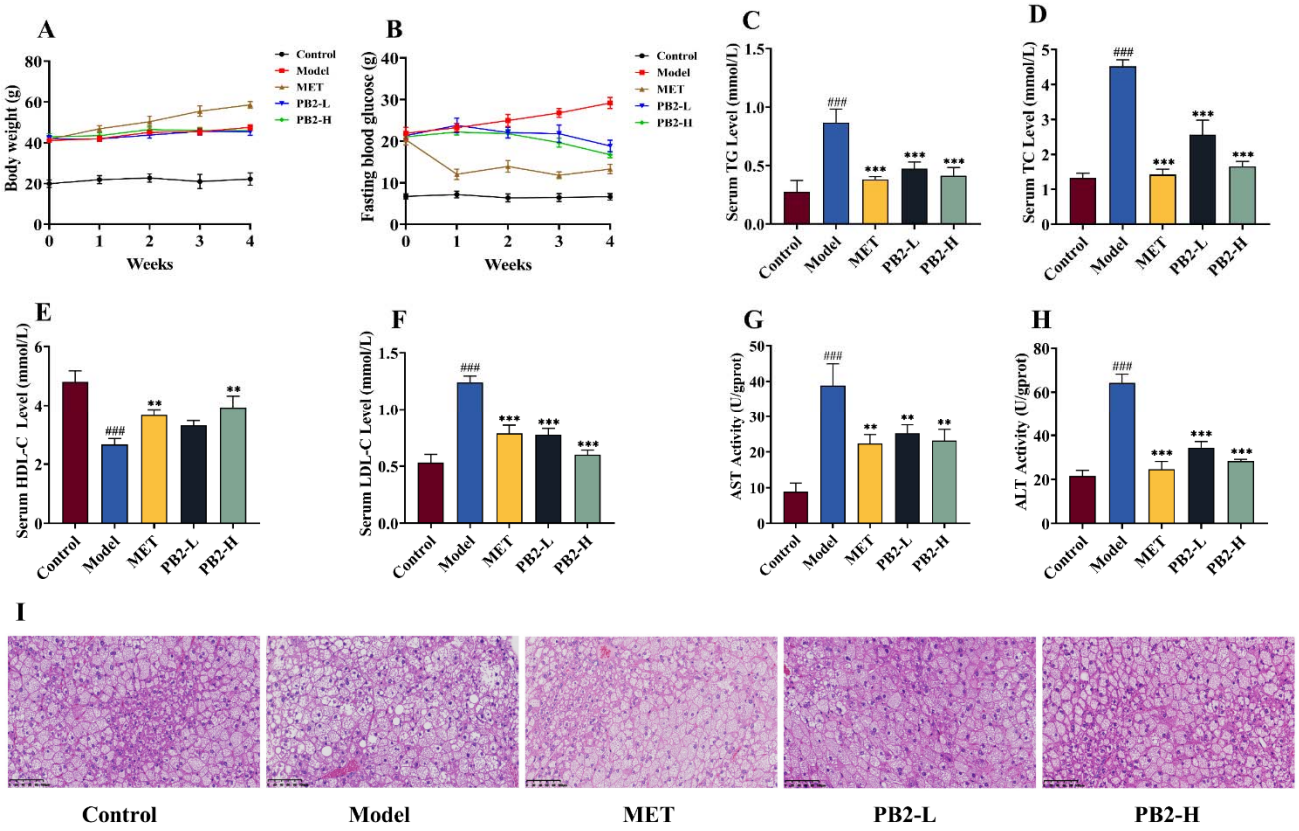

Figure 9. The effect of PB2 on physicochemical indicators and liver injury in *db/db* mice. (A) Body weight, (B) Fasting blood glucose (FBG), (C) Serum TG, (D) Serum TC, (E) Serum HDL-C, (F) Serum LDL-C, (G) AST, (H) ALT, (I) H&E staining of liver tissue sections (100×magnification). Data are expressed as mean ± SD (n≥3), $^{\#}P$ <0.05, $^{\#\#}P$ <0.01, $^{\#\#\#}P$ <0.001 vs. control group; $^{*}P$ <0.05, $^{**}P$ <0.01, $^{***}P$ <0.001 vs. model group.

3.11 The effect of PB2 on IR-related signaling pathways and redox balance in db/db mice

The regulatory effect of PB2 on insulin resistant-related signaling pathways was verified in liver tissue of *db/db* mice. As shown in Figure 10A-G, compared with the control group, the expression levels of key insulin-resistance-related proteins of p-IRS-1/IRS-1, p-AKT/AKT, p-GSK3β/GSK3β, and p-FoxO1/FoxO1 in the model group were significantly decreased (p<0.05, p<0.01, p<0.001), while the expression level of G6pase was significantly increased (p<0.001). After feeding with MET and PB2, the expressions of the above proteins were reversed; this may be achieved by promoting liver glycogen synthesis and inhibiting gluconeogenesis, which is keeping the accordance with that in cells as shown in Figure 4.

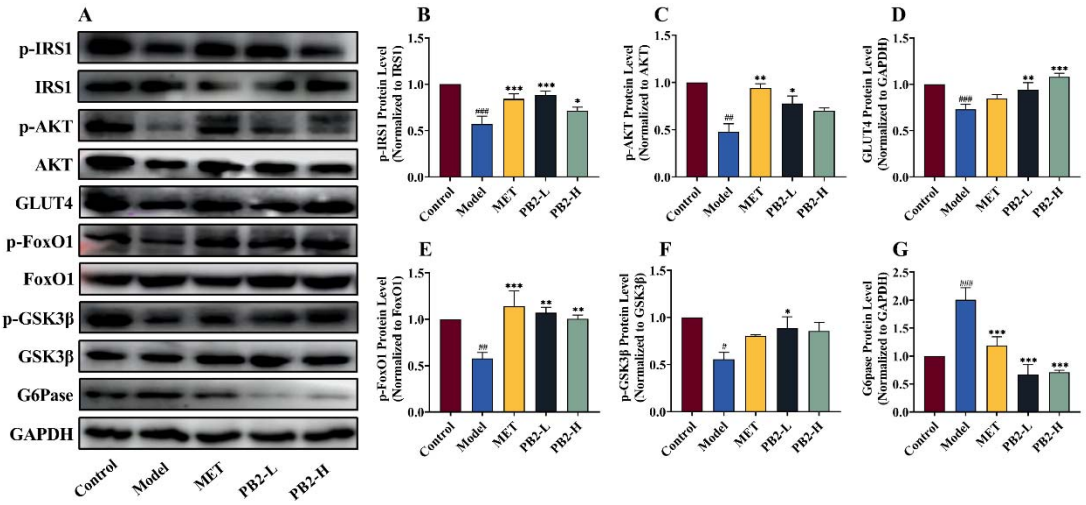

Figure 10. The regulatory effect of PB2 on protein expressions of insulin resistance signaling pathways in *db/db* mice. (A) Western blots of protein expressions by PB2 treatment. Relative protein expression ratios of (B) p-IRS1, (C) p-AKT, (D) GLUT4, (E) p-FoxO1, (F) p-GSK3β, and (G) G6pase in the liver tissues. Data are expressed as mean ± SD (n≥3), $^{\#}P$ <0.05, $^{\#\#}P$ <0.01, $^{\#\#\#}P$ <0.001 vs. control group; $^{*}P$ <0.05, $^{**}P$ <0.01, $^{***}P$ <0.001 vs. model group.

Similarly, the regulatory effect of PB2 on redox balance in *in vivo* level was further verified accordingly. As shown in Figure 11A-D, treatment with MET and PB2, MDA levels were significantly decreased (p<0.001), and expressions of SOD, CAT and GSH were significantly increased (p<0.05, p<0.01, p<0.001), which reversed the tendency from model group to control group. As shown in Figures 11E-H, MET and PB2 treatment significantly restored the expressions of Nrf2, HO-1, and NQO1 in the liver of *db/db* mice (p<0.05, p<0.01, p<0.001), compared with the control group. Therefore, these results indicated that PB2 could regulate redox balance in *db/db* mice by regulating the Nrf2 signaling pathway and thereby reducing oxidative stress-induced IR, which kept the accordance with that in cells as shown in Figure 5, too.

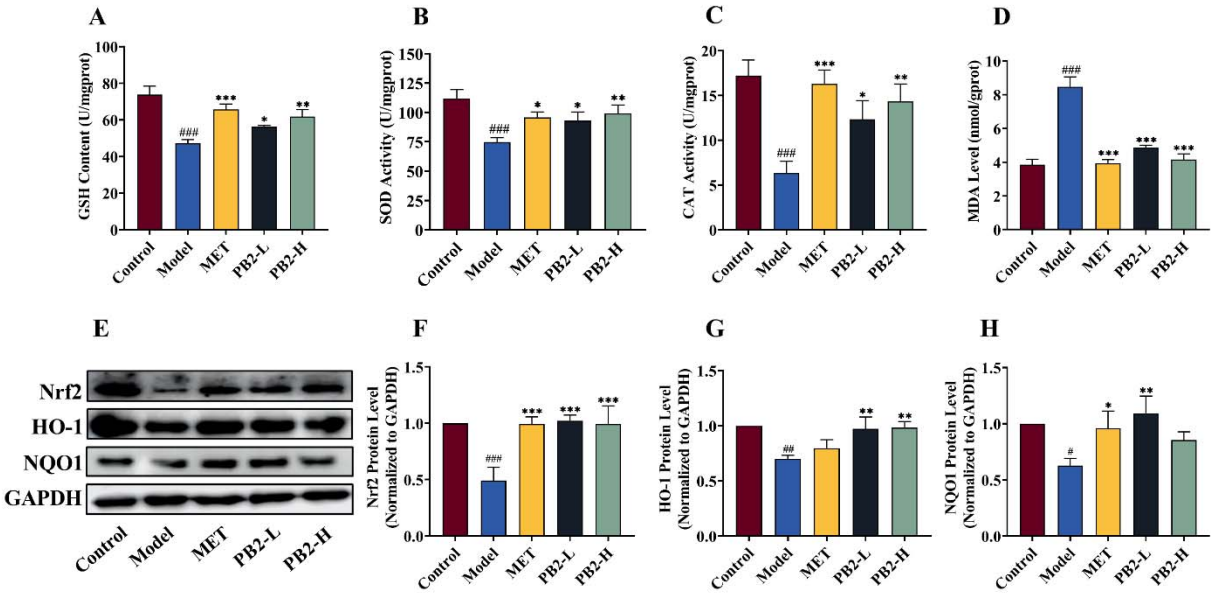

Figure 11. The effect of PB2 on oxidative stress and antioxidant signaling pathways in *db/db* mice. (A) GSH content. (B) SOD activity. (C) CAT activity. (D) MDA level. (E) Western blots of protein expressions by PB2 treatment. The relative protein expressions of (F) Nrf2, (G) HO-1, and (H) NQO1 in the liver tissues. Data are expressed as mean ± SD (n≥3), $^{\#}P$ <0.05, $^{\#\#}P$ <0.01, $^{\#\#\#}P$ <0.001 vs. control group; $^{*}P$ <0.05, $^{**}P$ <0.01, $^{***}P$ <0.001 vs. model group.

4. Discussion

IR is closely related to the progression of T2DM. It restricts insulin's function in facilitating glucose uptake and promoting lipid accumulation, and ultimately leads to hyperglycemia[28]. Several studies have demonstrated that a high-sugar environment induces oxidative stress, glucose metabolism disorders, and IR in HepG2 cells[29]. As a natural polyphenol plant compound, procyanidins have been extensively proven to exert beneficial effects on diabetes; however, research on the molecular mechanisms through which PB2 improves IR via blood glucose regulation remains limited.

Our research found that PB2 possesses antioxidant properties, with a stronger DPPH radical scavenging capacity than Trolox. PB2 also inhibited α-amylase and α-glucosidase; but its IC_{50} values for these enzymes were substantially higher than those of acarbose, indicating this inhibitory effect may play a secondary role in hypoglycemia. In contrast, activation of the IRS1/PI3K/AKT-Nrf2-GSK3β pathway was consistently observed, supporting this pathway as the primary mechanism underlying PB2-mediated IR improvement.

Network pharmacological results revealed that PB2 targets several key proteins, such as CASP3, MMP9, IGF1, AKT, and GSK3β. Among them, CASP3 is critical in diabetes and atherosclerosis, associated with pancreatic β-cell apoptosis and plaque progression[30]. IGF1 is closely related to the growth, differentiation, and insulin secretion of pancreatic-β cells[31]; and the MMP9 C(-1562)T gene polymorphism is linked to increased cardiovascular disease (CVD) risk in T2DM patients[32]. Furthermore, the PI3K/AKT and FoxO pathways were major routes for PB2 to counter IR. As a typical flavonoid, PB2's targeted proteins and signaling pathways align with previous studies on flavonoid-mediated regulation of abnormal glucose metabolism. For example, Xia et al. showed that coix polysaccharides treatment can regulate gut microbial composition, especially bacteria that generate short-chain fatty acids (SCFA), can activate the IGF1/PI3K/AKT pathway to exert hypoglycemic effects[33]. Ritu et al. found that the bioflavonoid combination, including ginger extract, soy extract, and hesperidin, alleviated diabetes-induced nephropathy in rats via modulation MMP-9/TIMP-1 expression, upregulated GLUT4, and downregulated TGF-β[34]. Zhang et al. reported that Huangbai Liniment can inhibit oxidative damage and apoptosis via Nrf2 pathway activation, enhance TGF-β1, reduce MMP9, and accelerate wound healing in diabetic[35]. Wu F et al. discovered that based on bioinformatics and transcriptomics studies that Huanglian-renshen-decoction can treat T2DM by suppressing hepatic glucose production, involving PI3K/AKT/FoxO1 pathway activation[36]. Deng et al. stated that water extract from artichoke (Cynara scolymus L.) can reduce the expression of PEPCK and G6Pase, and inhibit glycogen synthase (GS) phosphorylation, and alleviate palmitate-induced IR in HepG2 cells via IRS1/PI3K/AKT/FoxO1 and GSK3β pathway activation[37][36].

The *in vitro* experiments showed PB2 significantly increased glucose uptake and consumption in HepG2 cells compared to the model group, suggesting PB2 enhances glucose utilization to restore glucose metabolism and alleviate IR. PB2 also reduced MDA levels, suggesting its ability to alleviate oxidative stress and IR. Since the Nrf2 pathway serves as the primary cellular defense mechanism against oxidative stress[38], we investigated whether PB2 exerts antioxidant effects via this pathway. Results revealed that PB2

upregulates Nrf2, HO-1, and NQO1 expression, thereby stimulating antioxidant responses and increasing antioxidant enzymes, such as GSH and SOD. These findings suggested that PB2 alleviated oxidative stress by activating Nrf2-targeted pathways, which may further improve IR.

Numerous studies identify the PI3K/AKT pathway as a key regulator of glucose metabolism. IRS1 activates the PI3K/AKT signaling; as a downstream molecule of PI3K, activated AKT regulates glucose metabolism and improves IR by promoting glycogen synthesis and inhibiting gluconeogenesis[39][40]. Therefore, it plays a vital role in the development of diabetes, along with related renal damage and drug interventions. Some studies have shown that Nrf2 is located downstream of the PI3K/AKT pathway, and the PI3K/AKT can modulate the Nrf2 response to alleviate oxidative damage[41]. Further molecular data obtained in *in vitro* experiments demonstrated that PB2 also activated the PI3K/AKT and FoxO pathways, increasing GLUT4 and GSK3β expression to promote glycogen synthesis; it also promoted p-FoxO1 in liver cells and reduced G6Pase expression induced by high glucose, thereby inhibiting gluconeogenesis. These effects enhanced insulin sensitivity and improved the IR status of HepG2 cells. To investigate the relationship between PB2 and its potential to improve IR, we conducted molecular docking experiments. The molecular docking results showed that PB2 had low docking binding energy with AKT, Nrf2, GSK3β and FoxO1, in which GSK3β and AKT have stronger interactions with PB2, which indicated that PB2 may exert its IR improving ability via regulation of PI3K/AKT-Nrf2-GSK3β signaling, more than regulation of FoxO1 signaling pathway.

To delve deeper into the mechanisms by which the PI3K/AKT-Nrf2-GSK3β signaling cascade mediates therapeutic action of PB2 on IR, we treated cells to inhibitors targeting PI3K/AKT and Nrf2, thereby confirming the signaling interplay between PI3K/AKT and Nrf2. We observed that inhibitors of both PI3K/AKT and Nrf2 regulate the expression of GSK3β, promoting glycogen synthesis and inhibiting gluconeogenesis. This two-way regulatory mechanism suggests that PB2 may play a synergistic role in IR by activating the PI3K/AKT-Nrf2-GSK3β signaling axis. The siRNA technique, nucleocytoplasmic separation experiment, and pulldown technique were applied to deeply analyze the Nrf2-dependent regulatory mechanism and clarify the direct/indirect regulatory relationship of its downstream proteins on the IR pathway. Through docking analysis and GST-pull down verification, the direct physical binding between GSK3β and Nrf2 has been successfully found and identified.

The *in vivo* results in *db/db* mice confirmed that PB2 improved hyperglycemia, dyslipidemia, and liver oxidative stress, and upregulated the expression of key proteins in the IRS1/PI3K/AKT-Nrf2-GSK3β pathway in liver tissue. This consistency between *in vitro* and *in vivo* data strongly supports the reliability of the core mechanism and bridges the gap between cellular experiments and physiological conditions.

There are several limitations in the present study that should be noted and strengthened in the following studies. Firstly, only HepG2 liver cells were used to explore the mechanism of PB2 against IR. Although the liver is a core organ for glucose metabolism responsible for regulating glycogen synthesis, gluconeogenesis, and glucose output, it is important to recognize that IR is a systemic metabolic disorder requiring

coordination across multiple target tissues, such as adipose tissue and skeletal muscle. Future studies should verify the pathway in adipocytes or myotubes to confirm tissue-specific effects and fully elucidate PB2's systemic role in IR improvement. Although db/db mice validated the core pathway, the study did not investigate the pharmacokinetics of PB2 or its metabolites, and the contribution of PB2 metabolites to IR improvement remains unclear and will require further exploration. Specifically, multiple omics and artificial intelligence-aided precision nutritional methods or technologies are required to uncover the comprehensive molecular mechanism of PB2 and its original plants, due to the complexity of the multiple regulatory pathways, a series of biomarkers and the crosstalks with diabetes and other chronic diseases, such as hyperlipidemia， hyperuricemia， hypertension. Future studies could combine intestinal perfusion experiments to clarify the physiological relevance of this effect.

5. Conclusion

In the present study, the limited *in vitro* antioxidant activity and digestive enzyme inhibitory ability of PB2 encouraged the necessity to further investigate the regulatory effect of PB2 on glucose metabolism related signaling pathways at the cellular level. Network pharmacology analysis revealed that AKT and GSK3β were core targets and PI3K/AKT and FoxO were the main signaling pathways regulated by PB2 treatment against IR. Further molecular data indicated that PB2 improved high glucose-induced IR by enhancing glucose consumption and stimulating glycogen synthesis via modulation of PI3K/AKT-Nrf2-GSK3β signaling pathway, and successfully found and identified the direct bindings of PB2-Nrf2 and Nrf2-GSK3β. *In vivo* experiments using *db/db* mice further confirmed that PB2 exerted a hypoglycemic and IR-ameliorating effect by activating the PI3K/AKT-Nrf2-GSK3β signaling pathway. Collectively, this study identifies the PI3K/AKT-Nrf2-GSK3β pathway as a critical target for PB2-mediated IR improvement, providing evidence to support PB2's potential as a hypoglycemic agent or functional food component.

Funding

This work was supported by the grants from the National Key Research and Development Program of China (No. 2019YFC1604903) and the Hunan Natural Science Foundation (No. 2023JJ30295) to Si Qin, and partially supported by Natural Science Foundation of Hunan Province (No.2024JJ5225) to Tao Li and Excellent Youth Foundation of Education Department of Hunan Province (No. 23B0229) to Fangfang Yan.

Conflict of interest

We have no direct or indirect commercial financial incentive associated with publishing this article.

References

[1] M. P. CZECH. Insulin action and resistance in obesity and type 2 diabetes. Nature medicine. 23(7) (2017) 804-814. https://doi.org/10.1038/nm.4350.

[2] Q. NIE, J. HU, H. GAO, et al. Bioactive Dietary Fibers Selectively Promote Gut Microbiota to Exert Antidiabetic Effects. J Agric Food Chem. 69(25) (2021) 7000-7015. https://doi.org/10.1021/acs.jafc.1c01465.

[3] F. VALENZUELA ZAMUDIO, M. R. SEGURA CAMPOS. Amaranth, quinoa and chia bioactive peptides: a comprehensive review on three ancient grains and their potential role in management and prevention of Type 2 diabetes. Crit Rev Food Sci Nutr. 62(10) (2022) 2707-2721. https://doi.org/10.1080/10408398.2020.1857683.

[4] M. FENG, F. LIU, J. XING, et al. Anemarrhena saponins attenuate insulin resistance in rats with high-fat diet-induced obesity via the IRS-1/PI3K/AKT pathway. J Ethnopharmacol. 277 (2021) 114251. https://doi.org/doi:10.1016/j.jep.2021.114251.

[5] G. SOLINAS, B. BECATTINI. PI3K and AKT at the Interface of Signaling and Metabolism. Curr Top Microbiol Immunol. 436 (2022) 311-336. https://doi.org/doi:10.1007/978-3-031-06566-8_13

[6] Z. YANG, F. WU, Y. HE, et al. A novel PTP1B inhibitor extracted from Ganoderma lucidum ameliorates insulin resistance by regulating IRS1-GLUT4 cascades in the insulin signaling pathway. Food Funct. 9(1) (2018) 397-406. https://doi.org/doi:10.1039/c7fo01489a.

[7] D. E. JAMES, J. STöCKLI, M. J. BIRNBAUM. The aetiology and molecular landscape of insulin resistance. Nat Rev Mol Cell Biol. 22(11) (2021) 751-771. https://doi.org/ doi:10.1038/s41580-021-00390-6.

[8] T. JELENIK, K. KAUL, G. SéQUARIS, et al. Mechanisms of Insulin Resistance in Primary and Secondary Nonalcoholic Fatty Liver. Diabetes. 66(8) (2017) 2241-2253. https://doi.org/doi:10.2337/db16-1147.

[9] W. YU, C. CHEN, W. ZHUANG, et al. Silencing TXNIP ameliorates high uric acid-induced insulin resistance via the IRS2/AKT and Nrf2/HO-1 pathways in macrophages. Free Radic Biol Med. 178 (2022) 42-53. https://doi.org/doi:10.1016/j.freeradbiomed.2021.11.034.

[10] S. LI, N. EGUCHI, H. LAU, et al. The Role of the Nrf2 Signaling in Obesity and Insulin Resistance. Int J Mol Sci. 21(18) (2020) 6973. https://doi.org/doi:10.3390/ijms21186973.

[11] CM. DONADO-PESTANA, ÉVM. PESSOA, L. RODRIGUES, et al. Polyphenols of cambuci (Campomanesia phaea (O. Berg.)) fruit ameliorate insulin resistance and hepatic steatosis in obese mice. Food Chem. 340 (2021) 128169. https://doi.org/10.1016/j.foodchem.2020.128169.

[12] S. KUMAR, A. MITTAL, D. BABU, et al. Herbal Medicines for Diabetes Management and its Secondary Complications. Curr Diabetes Rev. 17(4) (2021) 437-56. https://doi.org/ 10.2174/1573399816666201103143225.

[13] X. P. WANG, Y. M. LI, Z. WANG, et al. [Advances of mechanism research on procyanidin in prevention and treatment of type 2 diabetes mellitus]. Zhongguo Zhong Yao Za Zhi. 42(20) (2017) 3866-3872. https://doi.org/10.19540/j.cnki.cjcmm.20170907.007.

[14] F. TIE, J. WANG, Y. LIANG, et al. Proanthocyanidins Ameliorated Deficits of Lipid Metabolism in Type 2 Diabetes Mellitus Via Inhibiting Adipogenesis and Improving Mitochondrial Function. Int J Mol Sci. 21(6) (2020) 2029. https://doi.org/10.3390/ijms21062029.

[15] F. FELDMAN, M. KOUDOUFIO, R. EL-JALBOUT, et al. Cranberry Proanthocyanidins as a Therapeutic Strategy to Curb Metabolic Syndrome and Fatty Liver-Associated Disorders. Antioxidants (Basel). 12(1) (2022) 90. https://doi.org/10.3390/antiox12010090.

[16] P. GONG, P. WANG, S. PI, et al. Proanthocyanidins Protect Against Cadmium-Induced Diabetic Nephropathy Through p38 MAPK and Keap1/Nrf2 Signaling Pathways. Front Pharmacol. 12 (2021) 801048. https://doi.org/10.3389/fphar.2021.801048.

[17] Y. W. XING, G. T. LEI, Q. H. WU, et al. Procyanidin B2 protects against diet-induced obesity and non-alcoholic fatty liver disease via the modulation of the gut microbiota in rabbits. World J Gastroenterol. 25(8) (2019) 955-966. https://doi.org/10.3748/wjg.v25.i8.955.

[18] L. HAN, L. L. ZHANG, W. F. MA, et al. Proanthocyanidin B2 attenuates postprandial blood glucose and its inhibitory effect on alpha-glucosidase: analysis by kinetics, fluorescence spectroscopy, atomic force microscopy and molecular docking. Food Funct. 9(9) (2018) 4673-4682. https://doi.org/10.1039/c8fo00993g.

[19] T. DAI, J. CHEN, Q. LI, et al. Investigation the interaction between procyanidin dimer and α-amylase: Spectroscopic analyses and molecular docking simulation. Int J Biol Macromol. 113 (2018) 427-433. https://doi.org/10.1016/j.ijbiomac.2018.01.189.

[20] X. LI, J. LIN, Y. GAO, et al. Antioxidant activity and mechanism of Rhizoma Cimicifugae. Chem Cent J. 6(1) (2012) 140. https://doi.org/10.1186/1752-153X-6-140.

[21] A. BHATNAGAR, R. SAINI, P. DAGAR, et al. Molecular modelling and in vitro studies of Daruharidra as a potent alpha-amylase inhibitor. J Biomol Struct Dyn. 41(9) (2023) 3872-3883. https://doi.org/10.1080/07391102.2022.2058093

[22] H. DING, X. HU, X. XU, et al. Inhibitory mechanism of two allosteric inhibitors, oleanolic acid and ursolic acid on α-glucosidase. Int J Biol Macromol. 107(Pt B) (2018) 1844-1855. https://doi.org/10.1016/j.ijbiomac.2017.10.040

[23] M. CAO, J. WANG, X. JIANG, et al. Phenolic Constituents from Black Quinoa Alleviate Insulin Resistance in HepG2 Cells via Regulating IRS1/PI3K/Akt/GLUTs Signaling Pathways. J Agric Food Chem. 71(48) 2023 18780-18791. https://doi.org/10.1021/acs.jafc.3c05900

[24] H.M. SU, Y.T. LI, D.W. HU, et al. Procyanidin B2 ameliorates free fatty acids-induced hepatic steatosis through regulating TFEB-mediated lysosomal pathway and redox state. Free Radical Biology and Medicine. 126 (2018) 269-286. https://doi.org/10.1016/j.freeradbiomed.2018.08.024

[25] J. FENG, C. WANG, T. LIU, et al. Procyanidin B2 inhibits the activation of hepatic stellate cells and angiogenesis via the Hedgehog pathway during liver fibrosis. Journal of Cellular and Molecular Medicine. 23(9) (2019) 6479-6493. https://doi.org/10.1111/jcmm.14543.

[26] M. KHALID, J. ALKAABI, M. A. B. KHAN, et al. Insulin Signal Transduction Perturbations in Insulin Resistance. International journal of molecular sciences. 22(16) (2021) 8590. https://doi.org/10.3390/ijms22168590.

[27] R. WU, T. JIAN, X. DING, et al. Total Sesquiterpene Glycosides from Loquat Leaves Ameliorate HFD-Induced Insulin Resistance by Modulating IRS-1/GLUT4, TRPV1, and SIRT6/Nrf2 Signaling Pathways. Oxidative medicine and cellular longevity. 2021 (2021) 4706410. https://doi.org/10.1155/2021/4706410.

[28] P. SAEEDI, I. PETERSOHN, P. SALPEA, et al. Global and regional diabetes prevalence estimates for 2019 and projections for 2030 and 2045: Results from the International Diabetes Federation Diabetes Atlas, 9 th edition. Diabetes research and clinical practice. 157 (2019) 107843. https://doi.org/10.1016/j.diabres.2019.107843.

[29] J. WANG, T. WU, L. FANG, et al. Peptides from walnut (Juglans mandshurica Maxim.) protect hepatic HepG2 cells from high glucose-induced insulin resistance and oxidative stress. Food & function. 11(9) (2020) 8112-8121. https://doi.org/10.1039/d0fo01753a.

[30] J. SUN, P. SINGH, J. ÖSTERLUND, et al. Hyperglycaemia-associated Caspase-3 predicts diabetes and coronary artery disease events. J Intern Med. 290(4) (2021) 855-865. https://doi.org/10.1111/joim.13327.

[31] L. LI, X. Y. MANG, K. W. JIANG, et al. Swimming training promotes angiogenesis of endothelial progenitor cells by upregulating IGF1 expression and activating the PI3K/AKT pathway in type 2 diabetic rats. Mol Med Rep. 30(6) (2024) 237. https://doi.org/10.3892/mmr.2024.13361.

[32] M. BURACZYNSKA, S. WRZOS, W. ZALUSKA. MMP9 Gene Polymorphism (rs3918242) Increases the Risk of Cardiovascular Disease in Type 2 Diabetes Patients. J Clin Med. 12(22) (2023) 6990. https://doi.org/10.3390/jcm12226990.

[33] T. XIA, C. S. LIU, Y. N. HU, et al. Coix seed polysaccharides alleviate type 2 diabetes mellitus via gut microbiota-derived short-chain fatty acids activation of IGF1/PI3K/AKT signaling. Food Res Int. 150(Pt A) (2021) 110717. https://doi.org/10.1016/j.foodres.2021.110717.

[34] Ritu, Y. XIONG, H. P. SHARMA, et al. Bioflavonoid combination attenuates diabetes-induced nephropathy in rats via modulation of MMP-9/TIMP-1, TGF-β, and GLUT-4-associated pathways. Heliyon. 10(13) (2024) e33217. https://doi.org/10.1016/j.heliyon.2024.e33217

[35] J. ZHANG, R. ZHOU, C. XIANG, et al. Huangbai Liniment Accelerated Wound Healing by Activating Nrf2 Signaling in Diabetes. Oxidative medicine and cellular longevity. 2020 (2020) 4951820. https://doi.org/10.1155/2020/4951820.

[36] F. WU, Q. SHAO, Q. XIA, et al. A bioinformatics and transcriptomics based investigation reveals an inhibitory role of Huanglian-Renshen-Decoction on hepatic glucose production of T2DM mice via PI3K/Akt/FoxO1 signaling pathway. Phytomedicine. 83 (2021) 153487. https://doi.org/10.1016/j.phymed.2021.153487.

[37] A. DENG, Y. WANG, K. HUANG, et al. Artichoke (Cynara scolymus L.) water extract alleviates palmitate-induced insulin resistance in HepG2 hepatocytes via the activation of IRS1/PI3K/AKT/FoxO1 and GSK-3β signaling pathway. BMC Complement Med Ther. 23(1) (2023) 460. https://doi.org/10.1186/s12906-023-04275-3.

[38] L. XU, N. NAGATA, T. OTA. Glucoraphanin: a broccoli sprout extract that ameliorates obesity-induced inflammation and insulin resistance. Adipocyte. 7(3) (2018) 218-225. https://doi.org/10.1080/21623945.2018.1474669.

[39] J. R. ROY, C. S. JANAKI, S. JAYARAMAN, et al. Effect of Carica papaya on IRS-1/Akt Signaling Mechanisms in High-Fat-Diet-Streptozotocin-Induced Type 2 Diabetic Experimental Rats: A Mechanistic Approach. Nutrients. 14(19) (2022) 4181. https://doi.org/10.3390/nu14194181.

[40] Y. YANG, W. LI, Y. LI, et al. Dietary Lycium barbarum polysaccharide induces Nrf2/ARE pathway and ameliorates insulin resistance induced by high-fat via activation of PI3K/AKT signaling. Oxidative medicine and cellular longevity. 2014 (2014) 145641. https://doi.org/10.1155/2014/145641.

[41] Y. HAO, Y. LI, J. LIU, et al. Protective Effect of Chrysanthemum morifolium cv. Fubaiju Hot-Water Extracts Against ARPE-19 Cell Oxidative Damage by Activating PI3K/Akt-Mediated Nrf2/HO-1 Signaling Pathway. Frontiers in nutrition. 8 (2021) 648973. https://doi.org/10.3389/fnut.2021.648973.